A complex point-source solution of the acoustic eikonal equation for Gaussian beams in transversely isotropic media

Running head: **Complex point-source solutions**

Xingguo Huang[1], Hui Sun[2,3], Zhangqing Sun[4] and Nuno Vieira da Silva[5]

[1] University of Bergen, Department of Earth Science, Allegaten 41, 5020 Bergen, Norway. Emails: Xingguo.Huang@uib.no,xingguo.huang19@gmail.com.

[2]Southwest Jiaotong University, Faculty of Geosciences and Environmental Engineering, Chengdu 610031, China; (Corresponding author) Email: sunhui@swjtu.edu.cn.

[3]University of California, Earth and Planetary Sciences, Modeling and Imaging Laboratory, 1156 High Street, Santa Cruz, CA 95064, USA.

[4]Jilin University, College for Geo-exploration Science and Technology, 938 Ximinzhu Street, Changchun 130026, China. Email: sun_zhangq@jlu.edu.cn.

[5]Formerly Imperial College London, Department of Earth Science and Engineering, South Kensington Campus, London SW7 2AZ, UK. Email: nuno.vdasilva@gmail.com.

ABSTRACT: The complex traveltime solutions of the complex eikonal equation are the basis of inhomogeneous plane-wave seismic imaging methods, such as Gaussian beam migration and tomography. We present the analytic approximations for complex traveltime in transversely isotropic media with a titled symmetry axis (TTI), which is defined by a Taylor series expansion over the anisotropy parameters. The formulation for complex traveltime is developed using perturbation theory and the complex point source method. The real part of the complex traveltime describes the wavefront and the imaginary part of the complex traveltime describes the decay of amplitude of waves away from the central ray. We derive the linearized ordinary differential equations for the coefficients of the Taylor-series expansion

using perturbation theory. The analytical solutions for the complex traveltimes are determined by applying the complex point source method to the background traveltime formula and subsequently obtaining the coefficients from the linearized ordinary differential equations. We investigate the influence of the anisotropy parameters and of the initial width of the ray tube on the accuracy of the computed traveltimes. The analytical formulas, as outlined, are efficient methods for the computation of complex traveltimes from the complex eikonal equation. In addition, those formulas are also effective methods for benchmarking approximated solutions.

INTRODUCTION

The complex eikonal equation plays an important role in wave propagation problems of inhomogeneous plane waves (Červený, 2001). The inhomogeneous plane wave is a solution of the elastodynamics equation if the traveltime is complex-valued (Krebes and Le, 1994). Studies on the complex eikonal equation fall into two groups. In the first group, the complex eikonal equation is used to describe the traveltimes in attenuating media. The complex eikonal equation is used for ray-based imaging and inversion (Huang et al, 2019) for an attenuating medium (i.e. the stiffness coefficients in the frequency-domain are complex-valued). Early studies on the complex traveltimes are based on the complex ray tracing method (Hearn and Krebes, 1990a, 1990b; Zhu and Chun, 1994; Thomson, 1997; Chapman et al., 1999; Kravtsov et al., 1990; Egorchenkov and Kravtsov, 2001). The computation of the complex ray tracing is very expensive because it is implemented in a high dimensional space. The introduction of the real ray tracing method based on perturbation theory (Vavryčuk, 2008a, 2008b, 2010, 2012; Klimeš and Klimeš, 2011) into the complex traveltimes computation enables computing complex traveltimes numerically.

The research work carried out in the 1980s is principally focused on developing a linear system of equations for asymptotic solutions concentrated in the vicinity of a ray utilizing a complex eikonal (Babich and Nomofilov, 1981; Nomofilov, 1982). That early reported work shows Hamiltonian formulations for the complex solution in some special systems of local coordinates. Although the theory is well established, numerical implementation for Hamiltonian formulations is not known. Effectively, solutions for Hamiltonian formulations require solving a system of differential equations numerically.

In the second group, the complex eikonal equation is used to describe the complex traveltimes of Gaussian beams. Since Deschamps's (1971), Wang and Deschamps' (1974) and Felsen's (1976) original formulations of the complex phase and the complex eikonal equation method, the complex traveltimes method has long attracted interest. Magnanini and Talenti (1999, 2003, 2006) use the Bäcklund transform to conduct some extensive research on the complex eikonal equation. The Bäcklund transform constitutes the basis of soliton theory (Terng and Karen, 2000). More recently, Li et al. (2011) develop a fast marching method to solve the complex eikonal equation without the limitation of the paraxial ray approximation. Accordingly, Huang et al. (2016b) design a local algorithm to compute the local complex traveltimes by combining the fast marching method with the nonuniform grid-based finite difference method. The complex traveltimes of the evanescent wave, in which their real part describes the wavefront while their imaginary part describes the decay away from the central ray, play an important role in local plane wave. Because of its advantages for handling caustics and multipath resulting from ray tracing in complex media, the complex traveltimes have been widely used for Gaussian beam modelling (Červený,

1982; Popov, 1982; Huang et al., 2016a; Huang, 2018) and seismic imaging (Hill, 1990, 2001; Gray, 2005, 2009).

The work outlined herein sits in the second group. In this paper, we focus on solving the Gaussian beam problem in a non-attenuating medium (i.e., the medium behaves elastically, and the stiffness coefficients are real-valued). We use a "real-valued" eikonal equation, but we force the traveltimes to be complex-valued, while Hearn and Krebs (1990a, 1990b), Zhu and Chun (1994), Thomson (1997), Chapman et al. (1999), Kravtsov et al. (1999), Egorchenkov and Kravtsov (2001) and Hao and Alkhalifah (2017a, b) use complex-valued eikonal equation without any enforcement of the traveltimes. Previously, the condition that the gradient of the real part of the traveltimes is orthogonal to that of the imaginary part is taken to solve the complex eikonal equation. That condition does not hold true for traveltimes determined from the complex eikonal equation for an attenuating isotropic medium. A key advantage of basing our discussion on Gaussian beam theory is that our expressions are readily applicable to complex heterogeneous media which is paramount for accurate seismic imaging (Hill, 2001).

When media are anisotropic, the isotropic approximation is no longer adequate (Huang and Greenhalgh, 2019). Areas with thin layering and fractures are particularly common in the geophysical exploration context, therefore the effect of anisotropy needs to be considered in realistic applications of the complex eikonal equation. This paper outlines the computation of the traveltimes for TTI media. Červený (2001) introduces the complex ray tracing method for general anisotropic elastic media. It is important to note that the application of such formulations is not usually feasible as the vast majority of the recorded datasets do not contain complete information on the elements of the full anisotropic stiffness tensor. In addition, it is unfeasible to consider the full anisotropic characterization of elastic media . It is often verified that disregarding shear waves from the constitutive law for an anisotropic medium yields an accurate representation of the kinematics of waves at the expense of sacrificing the accuracy of the computed amplitudes. However, it is important to note that modeling seismic waves with the true amplitude is generally not feasible as the exact source wavelet is unknown. In addition, the dynamic response of an acoustic medium is different from that of an elastic medium. The acoustic approximation has been widely used in seismic inversion and imaging (Alkhalifah, 2000, Grechka, 2004, Zhang et al., 2011, Duveneck and Bakker, 2011, da Silva et al, 2016). The work follows the same rationale regarding the constitutive law. The real eikonal approximation method is originally proposed as a means of computing the real-valued traveltimes for anisotropic media (Alkhalifah, 2011a, 2011b, 2013; Stovas and Alkhalifah, 2012; Waheed et al., 2013; Hao and Alkhalifah, 2017a, 2017b; Hao et al., 2018). In these methods, a Taylor expansion of the traveltimes with respect to the anisotropy parameters and to the background traveltimes for tilted elliptically isotropic media is carried out. The major advantage of these methods is that if we know the background traveltimes and anisotropy parameters, we can obtain traveltimes for general anisotropic media directly at a relatively low computational cost. More recently,

Huang et al. (2018) extend the mentioned above perturbation theory to the real and imaginary parts of the complex traveltimes, and they solve successfully the complex eikonal equation in VTI and orthorhombic media (Huang and Greenhalgh, 2018). Unlike the real eikonal approximation method, we take Taylor expansions of both the real and imaginary parts of the complex traveltimes. Then, we construct the linearized complex eikonal equations by substituting the Taylor's expansions into the complex eikonal equations.

According to the recent results of Huang et al. (2016b), solving the complex eikonal equation leads to an inverse process for computing the imaginary slowness. This process is especially complicated for anisotropic media. This is because the complex eikonal equation for anisotropic media includes several parameters: the normal moveout (NMO) velocity, velocity along the symmetry axis, and the anellipticity parameter, η.

This paper focus on two principal aspects. The first aspect is deriving the linearized complex eikonal equations based on perturbation theory (Alkhalifah, 2011a, 2011b, 2013; Stovas and Alkhalifah, 2012; Waheed et al., 2013; Hao et al., 2016; Hao and Alkhalifah, 2017a, 2017b; Hao et al., 2018). A key advantage of the linearized complex eikonal equations is providing possible method of solving the TTI complex eikonal equation using a finite-difference method, which can be used to address the computation of traveltimes in general heterogeneous media. Once the TTI complex eikonal equation can be solved directly, the paraxial ray approximation can be avoided while solving the complex eikonal equation. Following the recent methods (Huang and Greenhalgh, 2018; Huang et al., 2018), we develop a linear partial differential equation for the TTI complex eikonal equation. However, we use a tilted elliptically isotropic background medium for the perturbation expansion associated with the tilt angle, which allows us to perform the perturbation expansion in η only. This reduces uncertainty in the computed complex traveltimes.

The second aspect is obtaining the analytical formulas for homogeneous TTI media. The analytical solutions can be used to benchmark the accuracy of alternative methods, as well as, providing insight on the kinematics of wave propagation in TTI media. As pointed out earlier the latter has found many relevant applications in applied geophysics, especially in seismic imaging and inversion. Even though the theory developed in this paper applies to the general complex traveltimes for TTI media in the complex space, our closed form (analytical) solution is for a specific Gaussian beam. This is based on the fact that, for a complex point source (Choudhary and Felsen, 1974; Wang and Deschamps, 1974; Felsen, 1976, 1984; Wu, 1985), the beam has an initial constant phase front and a Gaussian field profile, and the wavefield has a Gaussian decay along the direction perpendicular to the central ray. In this case, the contours of the real part of the traveltimes define the equiphase contours, while the contours of the imaginary part define the phase paths. In addition, the theoretical development of the analytical formulas is based on another assumption that the distance is limited to the region of the paraxial ray approximation.

After defining the anisotropic complex traveltimes equation using the complex point source method, we substitute this equation into the linearized complex eikonal equations to obtain the coefficients of the Taylor expansions.

The analytical formulas of the complex travel time for TTI media based on the linearized complex eikonal equations are determined by introducing the complex point source method (Deschamps 1971; Felsen 1976, 1984) into the linearized complex eikonal method. However, it should be noted that although the linearized complex eikonal method in this paper is valid for an inhomogeneous background medium and an evanescent wave, the analytical formulas we will obtain are for a homogeneous medium and a specific Gaussian beam. In the following, we first describe the theory of constructing the complex eikonal equations for TTI media. Then based on perturbation theory, we introduce the linearized equations, followed by the analytical formulas for complex traveltimes of both the vertical and tilted rays in TTI media. Further, we demonstrate the effectiveness of the linearized complex eikonal method and the analytical formulas. Finally, we investigate the influence of locations, wave-width, and anisotropy parameters on the complex traveltimes.

COMPLEX EIKONAL EQUATIONS FOR INHOMOGENEOUS PLANE WAVES

In this section, we derive TTI complex eikonal equations in TTI media. As pointed out earlier the medium is considered acoustic and we only consider P-wave propagation. We depart from the eikonal equation introduced in Alkhalifah (2000)

$$(v_0)^2(1+2\eta)(\frac{\partial\tau}{\partial x})^2+(v_n)^2(\frac{\partial\tau}{\partial z})^2(1-2\eta(v_0)^2(\frac{\partial\tau}{\partial x})^2)=1. \tag{1}$$

where v_n is the vertical velocity, $v_0=v_n\sqrt{1+2\delta}$ is the NMO velocity, δ is the Thomsen's anisotropy parameter and η is the anellipticity parameter. The complex traveltimes τ can be expressed in terms of the real part τ_{R} and the imaginary part τ_{I}

$$\tau=\tau_{\mathrm{R}}+i\tau_{\mathrm{I}}\ , \tag{2}$$

where i represents the imaginary unit. Substituting equation 2 into equation 1, we obtain

$$\begin{aligned}&v_0^{\,2}(1+2\eta)((\frac{\partial\tau_R}{\partial x})^2-(\frac{\partial\tau_I}{\partial x})^2)+v_n^2(((\frac{\partial\tau_R}{\partial z})^2-(\frac{\partial\tau_I}{\partial z})^2)\\&(1-2\eta v_0^{\,2}((\frac{\partial\tau_R}{\partial x})^2-(\frac{\partial\tau_I}{\partial x})^2))+8\eta v_0^{\,2}\frac{\partial\tau_R}{\partial x}\frac{\partial\tau_I}{\partial x}\frac{\partial\tau_R}{\partial z}\frac{\partial\tau_I}{\partial z})-1=0\end{aligned}\ , \tag{3}$$

and

$$\begin{aligned}&2v_0^{\,2}(1+2\eta)\frac{\partial\tau_R}{\partial x}\frac{\partial\tau_I}{\partial x}+v_n^2(2(1-2\eta v_0^{\,2}((\frac{\partial\tau_R}{\partial x})^2-(\frac{\partial\tau_I}{\partial x})^2))(\frac{\partial\tau_R}{\partial z}\frac{\partial\tau_I}{\partial z})\\&-2\eta v_0^{\,2}((\frac{\partial\tau_R}{\partial z})^2-(\frac{\partial\tau_I}{\partial z})^2)(\frac{\partial\tau_R}{\partial x}\frac{\partial\tau_I}{\partial x}))=0\end{aligned}\ . \tag{4}$$

The rotation matrix for the complex eikonal equation from VTI media to TTI media is given by

$$L = \begin{bmatrix} \cos\theta & \sin\theta \\ -\sin\theta & \cos\theta \end{bmatrix} , \tag{5}$$

where θ is the angle between the symmetry axis and the vertical-axis. Substituting equation 5 to equations 3 and 4, we obtain the complex eikonal equations for TTI media

$$\begin{aligned} & v_0^2(1+2\eta)(G_R^2 - G_I^2) + v_n^2(F_R^2 - F_I^2)\left(1 - 2\eta^2 v^2 (G_R^2 - G_I^2) - 16\eta^2 v_0^4 G_R^2 G_I^2\right) \\ & +2\left\{\left[1 - 2\eta^2 v_0^2 (G_R^2 - G_I^2) - 16\eta^2 v_0^4 G_R^2 G_I^2\right] F_R F_I\right\} - 1 = 0 \end{aligned} , \tag{6}$$

and

$$2v_0^2(1+2\eta)G_R G_I - v_n^2 \begin{Bmatrix} 8\eta v_0^2 G_R G_I (F_R^2 - F_I^2)\left(1 - 2\eta^2 v_0^2 (G_R^2 - G_I^2)\right) + 16\eta v_0^2 \\ G_R G_I F_R F_I \left(1 - 2\eta^2 v_0^2 (G_R^2 - G_I^2)\right) \end{Bmatrix} = 0 . \tag{7}$$

where

$$\begin{aligned} G_R &= \cos\theta \frac{\partial \tau_R}{\partial x} + \sin\theta \frac{\partial \tau_R}{\partial z} \\ G_I &= \cos\theta \frac{\partial \tau_I}{\partial x} + \sin\theta \frac{\partial \tau_I}{\partial z} \end{aligned} , \tag{8}$$

and

$$\begin{aligned} F_R &= \cos\theta \frac{\partial \tau_R}{\partial z} - \sin\theta \frac{\partial \tau_R}{\partial x} \\ F_I &= \cos\theta \frac{\partial \tau_I}{\partial z} - \sin\theta \frac{\partial \tau_I}{\partial x} \end{aligned} . \tag{9}$$

In the case of $\eta = 0$, the TTI complex eikonal equations become the Tilted Elliptically Isotropic (TEI) complex eikonal equations

$$\begin{aligned} & v_0^2 \left[\left(\left(\frac{\partial \tau_R}{\partial x}\right)^2 - \left(\frac{\partial \tau_I}{\partial x}\right)^2 \right) \cos^2\theta - 2\left(\frac{\partial \tau_I}{\partial x}\frac{\partial \tau_I}{\partial z} - \frac{\partial \tau_R}{\partial x}\frac{\partial \tau_R}{\partial z} \right) \cos\theta \sin\theta \right. \\ & \left. + \left(\left(\frac{\partial \tau_R}{\partial z}\right)^2 - \left(\frac{\partial \tau_I}{\partial z}\right)^2 \right) \sin^2\theta \right] + v_n^2 \left[\left(\left(\frac{\partial \tau_R}{\partial z}\right)^2 - \left(\frac{\partial \tau_I}{\partial z}\right)^2 \right) \cos^2\theta \right. \\ & \left. + 2\left(\frac{\partial \tau_I}{\partial x}\frac{\partial \tau_I}{\partial z} - \frac{\partial \tau_R}{\partial x}\frac{\partial \tau_R}{\partial z} \right) \cos\theta \sin\theta + \left(\left(\frac{\partial \tau_R}{\partial x}\right)^2 - \left(\frac{\partial \tau_I}{\partial x}\right)^2 \right) \sin^2\theta \right] = 1 \end{aligned} , \tag{10}$$

and

$$\begin{aligned} & v_0^2 \left[\frac{\partial \tau_R}{\partial x}\frac{\partial \tau_I}{\partial x}\cos^2\theta + \frac{\partial \tau_R}{\partial z}\frac{\partial \tau_I}{\partial z}\sin^2\theta + \left(\frac{\partial \tau_R}{\partial x}\frac{\partial \tau_I}{\partial z} + \frac{\partial \tau_I}{\partial x}\frac{\partial \tau_R}{\partial z} \right) \cos\theta \sin\theta \right] \\ & + v_n^2 \left[\frac{\partial \tau_R}{\partial z}\frac{\partial \tau_I}{\partial z}\cos^2\theta + \frac{\partial \tau_R}{\partial x}\frac{\partial \tau_I}{\partial x}\sin^2\theta - \left(\frac{\partial \tau_R}{\partial x}\frac{\partial \tau_I}{\partial z} + \frac{\partial \tau_I}{\partial x}\frac{\partial \tau_R}{\partial z} \right) \cos\theta \sin\theta \right] . \\ & = 0 \end{aligned} \tag{11}$$

PERTURBATION THEORY

After obtaining the complex eikonal equation for TTI media, we can develop the linearized complex eikonal equations based on the perturbation method. Equations 6 and 7 are difficult to solve using a numerical method directly because of the large number of parameters and coupled real and imaginary parts. Thus, as in Alkhalifah (2011a, 2011b), and Stovas and Alkhalifah (2012), we expand the complex traveltime about the background complex travel time, with a Taylor series, for deriving the complex travel time for TTI media. Then the coefficients from the linearized complex eikonal equations can be used to calculate the whole complex travel time. For this purpose, following the same rationale as in Alkhalifah (2011b), we assume

$$\tau_R = \tau_{R0} + \tau_{R1}\eta + \tau_{R2}\eta^2 \ , \tag{12}$$

$$\tau_I = \tau_{I0} + \tau_{I1}\eta + \tau_{I2}\eta^2 \ , \tag{13}$$

where $\tau_{R0}(x,z)$ and $\tau_{I0}(x,z)$ are the real and imaginary parts of the complex traveltimes for the background media, respectively. These background complex traveltimes satisfy the TEI complex eikonal equations 10 and 11. For a matter of clarity, the coefficients of the linearized complex eikonal equations from a background elliptical anisotropy can be represented in vector notation to describe the tilt angles following Alkhalifah's approach (2011a). The components of that vector describe the projection of the symmetry axis on each plane.

COMPLEX ASYMPTOTIC SOLUTIONS USING COMPLEX POINT SOURCE METHODS

According to the research reported in Deschamps (1971) and in Felsen (1976, 1984), when the source of the wave is located at a complex point location, the angular spectrum of the wave is that of a plane wave whose wave vectors are close to the central ray. Thus, the theoretical development is based on the following assumptions: (1) the distance is limited to the region of the paraxial ray approximation, (2) the mathematical expressions are formulated in the acoustic approximation and (3) the angular spectrum of the wavefield has a Gaussian decay along the direction perpendicular to the central ray. It is necessary to use this approximation because the purpose of this work is to introduce an approximation of traveltimes for Gaussian beams. According to Felsen (1976, 1984) and to Wu (1985), the analytical solution in the paraxial region will be approximately equal to a Gaussian beam. The complex traveltimes computation method introduced in this paper is for Gaussian beams, which is effectively a kind of local plane wave. Thus, the complex traveltime, as outlined, gives a local traveltime along a single beam rather than a global traveltime. Huang et al. (2016a) introduce a local algorithm for computing local complex traveltimes.

According to the formulas for real eikonal equation (Golikov and Stovas, 2012), we give the

equation satisfying the complex eikonal equations 10 and 11 for tilted elliptically isotropic media

$$\tau_0(x,z)=\sqrt{\frac{\left(x-x_0\right)^2}{V^2}+\frac{(z-ib)^2}{V_t^2}} \quad , \tag{14}$$

where x_0 is the source position, with (Golikov and Stovas, 2012)

$$V_t^2=v_n^2\cos^2\theta+v_0{}^2\sin^2\theta \quad , \tag{15}$$

$$\frac{1}{V^2}=\frac{\cos^2\theta}{v_0{}^2}+\frac{\sin^2\theta}{v_n^2} \quad , \tag{16}$$

and

$$x_0=\frac{z\left(v_0{}^2-v_n^2\right)\sin\theta\cos\theta}{v_n^2\cos^2\theta+v_0{}^2\sin^2\theta} \quad , \tag{17}$$

where i represents the imaginary unit, and b is the initial width of the ray tube. Equation 14 is the formula for traveltimes in tilted elliptically isotropic media. That formula is obtained by setting the source point on the complex transverse plane. In equation 14, there is no angle parameter for the emitting direction of the ray. In fact, this means that the emitting angle is zero with z-axis.

Splitting equation 14 into its real and imaginary parts, applying the paraxial ray approximation (Wu, 1985) (The paraxial ray approximation is based on the assumption of $z^2>>x^2$ *and* $z^2>>b^2$.) and expanding with a Taylor-series expansion gives

$$\tau_0(x,z)=\frac{(z-ib)}{V_t}+\frac{\left(x-x_0\right)^2V_t}{2V^2(z-ib)} \quad . \tag{18}$$

Note that equation 18 is based on the Taylor-series expansion of equation, which suffers from a paraxial approximation assumption, meaning that it can only predict the traveltimes in the region in the vicinity of the central ray. Then, we divide equation 18 into real and imaginary parts, respectively:

$$\begin{aligned}\tau_{R0}(x,z)=\frac{1}{2}(&z\left(2b^2v^2-v_n^2x^2+2v_0{}^2z^2\right)\cos^3\theta-x\left(2b^2\left(v_0{}^2-v_n^2\right)+6v_0{}^2z^2+v_n^2\left(x^2-2z^2\right)\right)\\&\cos^2\theta\sin\theta+z\left(b^2v_n^2+6v_0{}^2x^2+v_n^2\left(-2x^2+z^2\right)\right)\cos\theta\sin^2\theta+x\left(b^2v_n^2-2v_0{}^2x^2-v_n^2z^2\right)\sin^3\theta)\\&/\left\{v_0{}^2v_n\left(\left(b^2+z^2\right)\cos^2\theta-2xz\cos\theta\sin\theta+x^2\sin^2\theta\right)\right\}\end{aligned} \quad , \tag{19}$$

and

$$\begin{aligned}\tau_{I0}(x,z)=\frac{1}{2}(&b\left(\left(2b^2v_0{}^2-v_n^2x^2+2v_0{}^2z^2\right)\cos^3\theta-4v_0{}^2xz\cos^2\theta\sin\theta\text{-}2v_t^2xz\sin^3\theta\right)\\&+\cos\theta\sin^2\theta\left(b^2v_n^2+2v_0{}^2x^2+v_n^2\left(-2x^2+z^2\right)\right))\\&/\left\{v_0{}^2v_n\left(\left(b^2+z^2\right)\cos^2\theta-2xz\cos\theta\sin\theta+x^2\sin^2\theta\right)\right\}\end{aligned} \quad . \tag{20}$$

The formulas above can be simplified by defining

$$\begin{aligned} X &= x\cos\theta + z\sin\theta \\ Z &= z\cos\theta - x\sin\theta \end{aligned}, \tag{21}$$

which is used to simplify the formulas in Appredix A. Substituting formulas 19 and 20 into equations A-1, A-2, A-9 and A-10, we obtain the coefficients of equations 12 and 13. Then, we can calculate the complex traveltimes of the vertical ray.

To improve the accuracy of the traveltimes computation, we use the first-sequence of the Shanks transform (Bender and Orszag, 1978)

$$\tau(x,z) \approx \frac{A_0 A_1 - A_1^2}{A_0 - 2A_1 + A_2}, \tag{22}$$

where

$$\begin{aligned} A_0 &= \tau_0 \\ A_1 &= \tau_0 + \tau_1\eta \\ A_2 &= \tau_0 + \tau_1\eta + \tau_2\eta^2 \end{aligned} \tag{23}$$

Details about the analytic approximations can be found in Appendix B.

To obtain the solutions when the ray is not vertical, one can transform the formulas above using coordinate transformation:

$$\begin{aligned} x' &= x\cos\varphi - z\sin\varphi \\ z' &= z\cos\varphi + x\sin\varphi \end{aligned}, \tag{24}$$

where φ is the angle of the ray with the vertical direction, and x' and z' are the transformed coordinates. It should be noted the properties for a tilted anisotropic medium are related to those of a respective canonical medium (local axis of symmetry) through a rotation transform, See Stovas and Alkhalifah (2012) and Ivanov and Stovas (2019) for more details on transverse isotropic and orthorhombic media, respectively. Figure 1 shows a schematic diagram for complex traveltime computation.

NUMERICAL RESULTS

Complex traveltimes of vertical beams in TTI media

First, to check the analytical formulas for the complex traveltimes presented here and to investigate the influence of anisotropy parameters η and δ on complex traveltimes, we show examples of the complex traveltimes of a vertical beam for TTI media with different parameters η. Figure 2 shows the complex traveltimes of a vertical beam for two anisotropic models ($6\text{ km}\times 6\text{ km}$). All models have the same velocity $v_0 = 2$ km/s, $\eta = 0.1$, $\delta = 0.05$; and $\theta = 10°$, but different anisotropy parameter η. The starting point of the ray is at (3 km, 0 km), and the initial width of the ray tube is 200m. Figures 2a and 2b show the real and imaginary parts of the complex traveltimes with the proposed method. Figures 2c and 2d

show the real and imaginary parts of the complex traveltimes with dynamic ray tracing. Figure 3 shows the comparison of complex traveltimes of a vertical beam with exact solutions (Huang et al., 2018b). The model size is $4\,\mathrm{km}\times 4\,\mathrm{km}$. The source is at (2 km, 2km). Figures 3e and 3f show the error of the real and imaginary parts, respectively. From Figures 3e and 3f, one can observe that the error is larger within the region around both sides of the source and far from the central ray. That is expected because the approximate solutions use the Taylor series expansion. All computations are performed with a processor Intel (R) Core (TM) i7-7700 CPU 3.60 GHz accessing 64 GB of RAM. The computational elapsed time for examples shown in Figures 2 and 3 are 45s and 48s, respectively.

Figure 4 shows the results with the same model as in Figure 2, except that the traveltimes are smoothed slightly, the tilt angle is $\theta = 5^\circ$ and the anellipticity parameter is $\eta = 0.05$. The most evident difference between Figures 2 and 4 is that the latter shows the complex traveltimes for a and b: $\delta = 0.1$; for c and d: $\delta = 0.2$. The starting point of the ray is located at (3 km, 0 km), and the initial width of ray tube is 300m. Figures 4a and 4c show the real part of the complex traveltimes, while Figures 4b and 4d show the imaginary part of the complex traveltimes.

From Figures 2 and 4, one can observe that (1) the contours of the real part of the complex traveltimes are approximately elliptical; (2) the contours of the imaginary part of the complex traveltimes are approximately hyperbolic; and (3) for the imaginary part of the complex traveltimes, there are some relatively large values in the top right region of the figures. This is because the imaginary part of the complex traveltimes is used to describe the increasing distance in the orthogonal direction to the central ray. The strength of the rays decreases with increasing distance from the central ray. It should be mentioned that the formulas are derived based on a paraxial approximation. This approximation is widely used in the field of ray theory. Huang and Greenhalgh (2018) and Huang et al. (2018) analyze the relative error of the approximate analytical formulas for orthorhombic (ORT) and VTI media. Because the region on the side of the source (the starting point of the central ray) is relatively far from the central ray, these values are relatively large. On the other hand, one can observe from Figures 4 and 5 that for the real part of the complex traveltimes, it is not symmetrical along the central ray. This is because the medium anisotropy affects the wavefront and the value of the angle θ is not zero. The comparison between the traveltimes computed utilizing the traveltime approximation and the dynamic ray tracing shows that the main difference occurs in the area around both sides of the source. That can be explained easily as unlike dynamic ray tracing, our approach uses the paraxial approximation which allows carrying out computations faster at the expense of some degree of inaccuracy. That leads to the inaccuracy of the formulas observed in the region of the source, where inaccuracies are more likely to occur due to the singular nature of the source point.

Complex traveltimes with different initial beam widths

Next, we compare the behavior of the complex traveltimes with different initial width of the ray tube. One can observe from equations 17 and 18 that the initial width of the tube is important to determine the behavior of the complex traveltimes. Figure 5 shows the complex traveltimes with the initial beam widths. The starting point of the ray is at (3 km, 0 km), while the initial widths of the ray tube are 200 m and 500 m, respectively. The size of the model is $6\ \text{km} \times 6\ \text{km}$. The model velocity is $v_0 = 2$ km/s, and the parameters of are $\eta = 0.1$, $\delta = 0.1$ and $\theta = 0.5$, respectively. Figures 5a and 5c show the real part of the complex traveltimes, while Figures 5b and 5d show the imaginary part of the complex traveltimes. Figure 6 shows a color plot of the complex traveltimes of a vertical beam for a TTI medium using the Shanks transform. From Figure 5, one can observe that the shape of the contours of the real part of the complex traveltimes with an initial ray tube width of 200 m are more similar to circles, whereas the shape of the contours of the imaginary part of the complex traveltimes with an initial ray tube width of 500m are more similar to ellipses. This is because the Gaussian beam is paraxially equivalent to a spherical wave with the center at the complex location. When the initial width of the ray tube is very small, it performs similarly to an approximated point source. Thus, the contours of the complex traveltimes look similar to circles. On the other hand, the difference between the traveltime plots for a width of 200 m and a width of 500 m can be noticeable. The difference is relatively large far from the source and in the region around both sides of the source. However, the strong similarity in shape suggests that the complex traveltimes retains the shape of the Gaussian beam and can be used to approximate the traveltimes of a beam.

Comparisons with elliptically isotropic media

We compare the traveltimes in isotropic media with that in anisotropic media, carrying out computations of the complex traveltimes. Figure 7 shows comparisons of the contours of the complex traveltimes of a vertical ray for the TTI model with the results for the elliptically isotropic model. The size of the model is $6\ \text{km} \times 6\ \text{km}$. The model velocity is $v_0 = 2$ km/s, and the anisotropy parameters are $\eta = 0.1$, $\theta = 5°$ and $\delta = 0.1$, respectively. The starting point of the ray is located at (3.5 km, 1 km). The green lines show the results for anisotropic media, and the red lines show the results for isotropic media. Figure 7a shows the real part of the complex traveltimes, and Figure 7b shows the imaginary part of the complex traveltimes. From Figure 7, one can observe that the contours of the real part of the complex traveltimes are approximately elliptical, whereas the contours of the imaginary part of the complex traveltimes are approximately hyperbolic. Figures 7c and 7d show the time differences between the TTI medium and the elliptically isotropic medium. This coincides with the distribution of the complex traveltimes based on Felsen's complex source point method (Felsen, 1976, 1984). From Figure 7, one also sees that there is some difference between the complex traveltimes for anisotropic media and

isotropic media. This difference is expected because complex traveltimes are affected by anisotropy. With the same real part of the complex traveltimes, the increase in the distance in anisotropic media is bigger than in isotropic media.

Influence of anisotropy on traveltimes

In this section, we investigate the influence of the medium anisotropy on the complex traveltimes at a fixed location point. To this end, we calculate the complex traveltimes for different changing anisotropy parameters. Figure 8 shows the influence of those parameters on the complex traveltimes. The size of the model is $6\ \text{km} \times 6\ \text{km}$. The location for Figures 8a and 8b is at (2 km, 2 km), and for Figures 8c and 8d is at (4 km, 4 km). The model velocity is $v_0 = 2\ \text{km/s}$, and the anisotropy parameters are $\eta = 0.3$, $\delta = 0.3$, respectively. The initial ray tube width is 300 m. Figures 8a and 8c show the influence of the anisotropic parameters on the real part of the complex traveltimes; while Figures 8b and 8d show the influence of the anisotropy parameters on the imaginary part of the complex traveltimes. The strong influence of the parameter of anisotropy δ on the complex traveltimes can be seen in Figures 8a and 8c. One can see that there is less influence of the anellipticity parameter η on the complex traveltimes than the anisotropy parameter δ. From Figures 8b and 8d, one can see that when the anellipticity parameter η is small while the anisotropic parameter δ is large, the complex traveltime is small. When the anellipticity parameter η is large while the anisotropic parameter δ is small, the complex traveltime difference is large. This means that the accuracy of the complex traveltimes depend on how well we obtain the anisotropic parameters. Because the traveltimes in anisotropic media depends on the anellipticity parameters η and δ, there are significant traveltimes differences with changes in η and δ. Both the real and imaginary parts vary significantly as a function of the anisotropy parameters. The contours of the real part of the traveltimes exhibit elliptical shapes, with big outer values and small inner values. The imaginary part of the traveltimes peaks at the large parameter η. Figure 9 shows color plot of the complex traveltimes associated with a tilted ray for an inhomogeneous VTI medium using the finite difference method (Huang et al., 2018). The size of the model is9 km $\times$ 9 km, which is based on the same model used in Figure 11 (Huang et al., 2018). The initial angle of the central ray is $\theta = 60°$. The starting point of the central ray is at (4.5 km, 300m), and the initial beam width is 500 m. Figure 9a shows the velocity model, Figure 9b shows δ model, Figure 9c shows ε model, Figure 9d shows the real part of the complex traveltimes and Figure 9e shows the imaginary part of the complex traveltimes. The computational time is 3643 s. This example demonstrates that the derived differential equations can be not only used for homogeneous media but also for inhomogeneous media.

DISCUSSIONS

The most important contribution of the paper is to derive the analytic approximations for complex traveltime in transversely isotropic media with a titled symmetry axis (TTI) using perturbation theory and the complex point source method. Those formulas are also effective methods for benchmarking numerical solutions in such media and investigating seismic anisotropy. In addition, to develop the approximate solutions, we derive the complex eikonal equation for inhomogeneous waves in TTI media. Then we transform the nonlinear compelx eikonal equation into the linearized ordinary differential equations that can be solved by the farst marching method and finite difference method numerically.

In theory, the complex point source analytic continuation, and the analysis into the spaces of complex distances can provide exact Green's function. From the practical point of view, the 2D complex point source Green's function provides a frequency-independent formulation, and not only under high-frequency asymptotic approximation. This exact solution, and the complex analysis associated to it thus become a reference standard for the analysis and comparison of other practical and very important solutions obtained under certain approximations. The formulas for the complex traveltime derived in this paper use second-order approximations rather than first-order. Although the complex approximation solution is not the more efficient from a practical point of view, it constitutes a reference standard against which other formulations and approximations may be qualitatively compared.

Actually, there are several reasons to investigate such asymptotic solutions. Theoritically, the approximate solution provides a description of propagation of the inhomogeneous waves. The complex eikonal equation plays an important role in wave propagation problems of inhomogeneous plane waves, which gives asymptotic solutions concentrated in the vicinity of a ray utilizing a complex eikonal. One main reason why we need the high-frequency asymtotic solutions is that we can investigate wave propagation phenemonon and separate the propagation events into reflection and refraction, etc. From application perspective, the complex approximate solution can be used for Gaussian beams, which are widely used for seismic modeling and imaging. Actually, because of its advantages for handling caustics and multipath resulting from ray tracing in complex media, the complex traveltimes have been widely used for Gaussian beam modelling in the past decades. Another reason is that the formulations provide anisotropy parameter estimation capabilities for a general inhomogeneous background medium. This is practical since conventional seismic experiments combined with well information may provide us with a background elliptically anisotropic inhomogeneous model. An extension to more "real world" 3D TTI or tilted orthorhombic problems even 3D elastic case is easy and realstic. For 3D TI media with a tilt in the axis of symmetry, two additional parameters θ and φ that describe the tilt in three dimensions are needed to fully characterize a high-frequency acoustic wave propagation. Expanding the complex traveltime solutions of the complex eikonal equation in a power series in terms of the independent

anisotropic parameter and aplying the complex sourse point leads to the complex approximate solutions.

Here, we give some explanations why we need such a approximate solution rather than we use a GPU to compute full wavefield solutions of 2D elastodynamic equation. It is beyond doubt that indeed there has been a significant progress in the past years. The 2D wave simulation with GPU cards can be carried out significantly faster than before. In 3D the FD computational cost increases by a factor of at least 8 times compared to that of 2D. For large scale applications it starts hitting limitations in the GPU's cache and that requires very specific programming techniques to avoid any issues. Basically our point is that comparing a FD computing on a GPU against our implementation is not an entirely "apples to apples" comparison. However, if we want to extract maximum capability of hardware, then we can argue that we could use a GPU implementation of our method and likely simulate an entire 2D survey with a run-time similar to that it would take a GPU to simulate a shot gather. The reason is because, with our current implementation, we are getting a comparable run-time by just using a single core.

We also point out indeed nowadays we are simulating wave equations at higher and higher frequencies. However, even these days RTM is generally not run at full-bandwidth and in fact 60-70 Hz really is the upper limit in the vast majority of commercial applications. This is the reason why many RTM images seem to have lower spectral content than the Kirchhoff counterparts. In fact Kirchhoff migration is still a must in seismic imaging. And with Kirchhoff migration we also include Gaussian beam migration which finds a wide range of applications. We point out that these methods (Gaussian Beam Migration and Kirchhoff) are heavily based on computing traveltimes with ray-based theory. Hence, the proposed method finds applicability in a vast domain of application and for that reason we also believe that our approach is relevant.

CONCLUSIONS

We have presented the analytical solutions for the computation of complex traveltimes with the complex eikonal equation for TTI media. The complex eikonal equation is derived assuming that the complex traveltimes for TTI media can be expanded in a Taylor series. As a result, we obtain linearized ordinary differential equations for the coefficients, which can be used to construct the complex traveltime formulas. The complex point source method plays an important role in developing those analytical solution. The paraxial approximation and background complex traveltimes are required for solving the TTI complex eikonal equation. However, if the aim of solving the TTI complex eikonal equation is to compute the seismic complex traveltimes, then we can only compute a special case of the Gaussian beam. Compared to the dynamic ray tracing method, the method outlined in this paper has higher efficiency because it is based on an analytical solution. The method presented herein is therefore a closed form solution for the computation of complex traveltimes. It is useful for benchmarking alternative numerical approaches, including methods based upon ray theory, or explicit discretization of wave equations for

acoustic media with transverse isotropy, which are adequate for heterogeneous media. The expressions derived and discussed herein are based on the theory of Gaussian beams. They can then be used for the computation of multi-traveltime arrivals which find application in seismic imaging and inversion in heterogeneous media. Applying the equations introduced herein to those media is straightforward requiring their discretization with numerical methods, such as the finite-difference method. The approach outlined herein can be used for both homogeneous and inhomogeneous media. However, the method is based on perturbation theory, which assumes small perturbation in the variables. Thus, this method is not adequate for the computation of complex traveltimes in media with strongly velocity variation. Due to the use of the paraxial approximation in the derivation of the equations, the propagation accuracy decreases when the beam width is too large. That means that one can only calculate the local complex traveltimes in the region close to the central ray. Due to its characteristics, we find application in seismic imaging especially in Gaussian beam migration which is conforming with the criteria for selecting the initial width of the ray.

APPENDIX A: LINEAR PARTIAL DIFFERENTIAL EQUATIONS FOR THE COEFFICIENTS OF TAYLOR SERIES EXPANSION

In this appendix, we derive the linear partial differential equations for the coefficients of Taylor expansion. These equations are the basis to develop analytic traveltime approximations. When substituting equations 19 and 20 into equations 13 and 14, we have the complex coefficients in η

$$\left[\left(\tau_{R0,x}\tau_{R1,x}-\tau_{I0,x}\tau_{I1,x}\right)v_0^{\,2}+\left(\tau_{R0,z}\tau_{R1,z}-\tau_{I0,z}\tau_{I1,z}\right)v_n^2\right]\cos^2\theta-\left(\tau_{I0,z}\tau_{I1,x}+\tau_{I0,x}\tau_{I1,z}-\tau_{R0,z}\tau_{R1,x}-\tau_{R0,x}\tau_{R1,z}\right)$$
$$\times\left(v_0^{\,2}-v_n^2\right)\cos\theta\sin\theta+\left[\left(\tau_{R0,z}\tau_{R1,z}-\tau_{I0,z}\tau_{I1,z}\right)v_0^{\,2}+\left(\tau_{R0,x}\tau_{R1,x}-\tau_{I0,x}\tau_{I1,x}\right)v_n^2\right]\sin^2\theta=Q_{R1}$$
, (A-1)

and

$$\left[\left(\tau_{R0,x}\tau_{R1,x}+\tau_{I0,x}\tau_{I1,x}\right)v_0^{\,2}+\left(\tau_{R0,z}\tau_{R1,z}+\tau_{I0,z}\tau_{I1,z}\right)v_n^2\right]\cos^2\theta+\left(\tau_{R0,z}\tau_{I1,x}+\tau_{R0,x}\tau_{I1,z}+\tau_{I0,z}\tau_{R1,x}+\tau_{I0,x}\tau_{R1,z}\right)$$
$$\times\left(v_0^{\,2}-v_n^2\right)\cos\theta\sin\theta+\left[\left(\tau_{R0,z}\tau_{I1,z}+\tau_{I0,z}\tau_{R1,z}\right)v_0^{\,2}+\left(\tau_{R0,x}\tau_{I1,x}+\tau_{I0,x}\tau_{R1,x}\right)v_n^2\right]\sin^2\theta=Q_{I1}$$
, (A-2)

where

$$Q_{R1}=-v_n^2\left(G_{R0}^2-G_{I0}^2\right)+v_n^2v^2\left[\left(G_{R0}^2-G_{I0}^2\right)\left(F_{R0}^2-F_{I0}^2\right)-4G_{R0}G_{I0}F_{R0}F_{I0}\right]\ , \tag{A-3}$$

and

$$Q_{I1}=-2v_n^2G_{R0}G_{I0}+v_n^2v_0^{\,2}\left[2G_{R0}G_{I0}\left(F_{R0}^2-F_{I0}^2\right)+2F_{R0}F_{I0}\left(G_{R0}^2-G_{I0}^2\right)\right]\ , \tag{A-4}$$

with

$$\begin{aligned}G_{R0}&=\cos\theta\frac{\partial\tau_{R0}}{\partial x}+\sin\theta\frac{\partial\tau_{R0}}{\partial z}\\ G_{I0}&=\cos\theta\frac{\partial\tau_{I0}}{\partial x}+\sin\theta\frac{\partial\tau_{I0}}{\partial z}\end{aligned}\ , \tag{A-5}$$

$$\begin{aligned}G_{R1}&=\cos\theta\frac{\partial\tau_{R1}}{\partial x}+\sin\theta\frac{\partial\tau_{R1}}{\partial z}\\ G_{I1}&=\cos\theta\frac{\partial\tau_{I1}}{\partial x}+\sin\theta\frac{\partial\tau_{I1}}{\partial z}\end{aligned}\ , \tag{A-6}$$

$$\begin{aligned}F_{R0}&=\cos\theta\frac{\partial\tau_{R0}}{\partial z}-\sin\theta\frac{\partial\tau_{R0}}{\partial x}\\ F_{I0}&=\cos\theta\frac{\partial\tau_{I0}}{\partial z}-\sin\theta\frac{\partial\tau_{I0}}{\partial x}\end{aligned}\ , \tag{A-7}$$

$$\begin{aligned}F_{R1}&=\cos\theta\frac{\partial\tau_{R1}}{\partial z}-\sin\theta\frac{\partial\tau_{R1}}{\partial x}\\ F_{I1}&=\cos\theta\frac{\partial\tau_{I1}}{\partial z}-\sin\theta\frac{\partial\tau_{I1}}{\partial x}\end{aligned}\ , \tag{A-8}$$

where

$$\tau_{R0,x}=\frac{\partial\tau_{R0}}{\partial x},\tau_{R0,z}=\frac{\partial\tau_{R0}}{\partial z},\tau_{I0,x}=\frac{\partial\tau_{I0}}{\partial x},\tau_{I0,z}=\frac{\partial\tau_{I0}}{\partial z},\tau_{R1,x}=\frac{\partial\tau_{R1}}{\partial x},\tau_{R1,z}=\frac{\partial\tau_{R1}}{\partial z},\tau_{I1,x}=\frac{\partial\tau_{I1}}{\partial x},\tau_{I1,z}=\frac{\partial\tau_{I1}}{\partial z}.$$

The complex coefficients of second power in η^2 are written as

$$\begin{aligned}&-2(\cos\theta^2\left[\tau_{I0,x}\tau_{I2,x}{v_0}^2-\tau_{R0,x}\tau_{R2,x}{v_0}^2+\left(\tau_{I0,z}\tau_{I2,z}-\tau_{R0,z}\tau_{R2,z}\right)v_n^2\right]+\left(\tau_{I0,z}\tau_{I2,x}+\tau_{I0,x}\tau_{I2,z}-\tau_{R0,z}\tau_{R2,x}-\tau_{R0,x}\tau_{R2,z}\right)\\&\times\left({v_0}^2-v_n^2\right)\cos\theta\sin\theta+\left[\tau_{I0,z}\tau_{I2,z}v^2-\tau_{R0,z}\tau_{R2,z}{v_0}^2+v_n^2\left(\tau_{I0,x}\tau_{I2,x}-\tau_{R0,x}\tau_{R2,x}\right)\right]\sin\theta^2)=Q_{R2}\end{aligned}$$

(A-9)

and

$$\begin{aligned}&-(\left(\tau_{R0,x}\tau_{I2,x}{v_0}^2+\tau_{I0,x}\tau_{R2,x}{v_0}^2+\left(\tau_{R0,z}\tau_{R2,z}+\tau_{I0,z}\tau_{R2,z}\right)v_n^2\right)\cos^2\theta\\&+\left(\tau_{R0,z}\tau_{I2,x}+\tau_{R0,x}\tau_{I2,z}+\tau_{I0,z}\tau_{R2,x}+\tau_{I0,x}\tau_{R2,z}\right)\left({v_0}^2-v_n^2\right)\cos\theta\sin\theta\\&+\left(\tau_{I0,z}\tau_{R2,z}{v_0}^2+\left(\tau_{R0,x}\tau_{I2,x}+\tau_{I0,x}\tau_{R2,x}\right)v_n^2+\tau_{R0,z}\tau_{I2,z}{v_0}^2\right)\sin^2\theta)=Q_{I2}\end{aligned},\qquad\text{(A-10)}$$

where

$$\begin{aligned}Q_{R2}&=-v_n^2\left(F_{R1}^2+F_{I1}^2\right)-{v_0}^2\left(G_{R1}^2-G_{I1}^2+4G_{R0}G_{R1}-4G_{I0}G_{I1}\right)\\&+4{v_0}^2v_n^2\left[\left(G_{R0}^2-G_{I0}^2\right)\left(F_{R0}F_{R1}+F_{I0}F_{I1}\right)-2G_{R0}G_{I0}\left(F_{I0}F_{R1}+F_{R0}F_{I1}\right)\right]\end{aligned},\qquad\text{(A-11)}$$

and

$$\begin{aligned}Q_{I2}&=-2v_n^2F_{R1}F_{I1}-{v_0}^2\left(2G_{R1}G_{I1}+4G_{R0}G_{I1}+4G_{I0}G_{R1}\right)\\&+4{v_0}^2v_n^2\left[\left(G_{R0}^2-G_{I0}^2\right)\left(F_{I0}F_{R1}+F_{R0}F_{I1}\right)+2G_{R0}G_{I0}\left(F_{R0}F_{R1}-F_{I0}F_{I1}\right)\right]\end{aligned},\qquad\text{(A-12)}$$

where $\tau_{R2,x}=\frac{\partial\tau_{R2}}{\partial x},\tau_{R2,z}=\frac{\partial\tau_{R2}}{\partial z},\tau_{I2,x}=\frac{\partial\tau_{I2}}{\partial x},\tau_{I2,z}=\frac{\partial\tau_{I2}}{\partial z}$.

APPENDIX B: THE APPROXIMATE ANALYTIC SOLUTIONS

In this section, we give the approximate analytic traveltime formulas. We start with the analytic formulas for the background medium. The equation satisfying the complex eikonal equations 17 and 18 in tilted elliptically isotropic media is given by

$$\tau_0(x,z)=\sqrt{\frac{\left(x-x_0\right)^2}{V^2}+\frac{(z-ib)^2}{V_t^2}} \quad , \tag{B-1}$$

where

$$V_t^2=v_n^2\cos^2\theta+{v_0}^2\sin^2\theta \quad , \tag{B-2}$$

$$\frac{1}{V^2}=\frac{\cos^2\theta}{{v_0}^2}+\frac{\sin^2\theta}{v_n^2} \quad , \tag{B-3}$$

$$x_0=\frac{z\left({v_0}^2-v_n^2\right)\sin\theta\cos\theta}{v_n^2\cos^2\theta+{v_0}^2\sin^2\theta} \quad . \tag{B-4}$$

Substituting equations B-1, B-2 and B-3 into equation B-1, using the Taylor expansion, we obtain

$$\tau_{R0}(x,z)=\frac{1}{2}\frac{z\left(2b^2{v_0}^2-v_n^2x^2+2{v_0}^2z^2\right)\cos^3\theta-x\left(2b^2\left({v_0}^2-v_n^2\right)+6{v_0}^2z^2+v_n^2\left(x^2-2z^2\right)\right)\cos^2\theta\sin\theta}{{v_0}^2v_n\left(\left(b^2+z^2\right)\cos^2\theta-2xz\cos\theta\sin\theta+x^2\sin^2\theta\right)}$$
$$+\frac{z\left(b^2v_n^2+6{v_0}^2x^2+v_n^2\left(-2x^2+z^2\right)\right)\cos\theta\sin^2\theta+x\left(b^2v_n^2-2{v_0}^2x^2-v_n^2z^2\right)\sin^3\theta}{{v_0}^2v_n\left(\left(b^2+z^2\right)\cos^2\theta-2xz\cos\theta\sin\theta+x^2\sin^2\theta\right)} \quad , \tag{B-5}$$

and

$$\tau_{I0}(x,z)=\frac{1}{2}\frac{b\left[\left(2b^2{v_0}^2-v_n^2x^2+2{v_0}^2z^2\right)\cos^3\theta-4v^2xz\cos^2\theta\sin\theta-2v_n^2xz\sin^3\theta\right]}{{v_0}^2v_n\left(\left(b^2+z^2\right)\cos^2\theta-2xz\cos\theta\sin\theta+x^2\sin^2\theta\right)}$$
$$+\frac{\left(b^2v_n^2+2{v_0}^2x^2+v_n^2\left(-2x^2+z^2\right)\right)\cos\theta\sin^2\theta}{{v_0}^2v_n\left(\left(b^2+z^2\right)\cos^2\theta-2xz\cos\theta\sin\theta+x^2\sin^2\theta\right)} \quad . \tag{B-6}$$

When substituting equations B-5 and B-6 into equations A-1 and A-2, we have

$$\tau_{R1}(x,z)=\tau_{R1F}(x,z)\tau_{R0}(x,z)-\tau_{I1F}(x,z)\tau_{I0}(x,z) \quad , \tag{B-7}$$

and

$$\tau_{I1}(x,z)=\tau_{R1F}(x,z)\tau_{I0}(x,z)+\tau_{I1F}(x,z)\tau_{R0}(x,z) \quad , \tag{B-8}$$

where

$$\tau_{R1F} = \frac{\tau_{R1U1} + \tau_{R1U2}}{\tau_{1D}} \quad , \tag{B-9}$$

and

$$\tau_{I1F} = \frac{\tau_{I1U}}{\tau_{1D}} \quad , \tag{B-10}$$

where

$$\begin{aligned}\tau_{R1U1} = -(&v_n^4(v_0{}^4\left(b^2\sin^2\theta + X^2\right)^4 + 2v_0{}^2v_n^2\left(b^2\sin^2\theta + X^2\right)^2(b^4\cos^2\theta\sin^2\theta + X^2Z^2 \\ &-b^2\left(\cos^2\theta X^2 - 4\cos\theta\sin\theta XZ + \sin^2\theta Z^2\right)))\end{aligned} \quad , \tag{B-11}$$

$$\begin{aligned}\tau_{R1U2} = -\{&v_n^4\{b^8\cos^4\theta\sin^4\theta + X^4Z^4 - 2b^6\cos^2\theta\sin^2\theta\left[3\cos^2\theta X^2 - 8\cos\theta\sin\theta XZ + 3\sin^2\theta Z^2\right] \\ &-2b^2X^2Z^2\left(3\cos^2\theta X^2 - 8\cos\theta\sin\theta XZ + 3\sin^2\theta Z^2\right) \\ &+b^4\left[\cos^4\theta X^4 - 16\cos^3\theta\sin\theta X^3Z + 36\cos^2\theta\sin^2\theta X^2Z^2 - 16\cos\theta\sin^3\theta XZ^3 + \sin^4\theta Z^4\right]\}\}\end{aligned} \quad , \tag{B-11}$$

and

$$\begin{aligned}\tau_{1D} = \{&v_0{}^4\left(b^2\sin^2\theta + X^2\right)^2 + \left(b^2\cos^2\theta + Z^2\right)^2v_n^4 \\ &+2v_0{}^2v_n^2\left[b^4\cos^2\theta\sin^2\theta + X^2Z^2 - b^2\left(\cos^2\theta X^2 - 4\cos\theta\sin\theta XZ + \sin^2\theta Z^2\right)\right]\}^2\end{aligned} \quad , \tag{B-12}$$

and

$$\begin{aligned}\tau_{I1U} = 4\{&b\left(\cos\theta X - \sin\theta Z\right)\left(b^2\cos\theta\sin\theta + XZ\right)v_n^6v^2\left(b^2\sin^2\theta + X^2\right)^2 \\ &+\left(b^4\cos^2\theta\sin^2\theta + X^2Z^2 - b^2\left(\cos^2\theta X^2 - 4\cos\theta\sin\theta XZ + \sin^2\theta Z^2\right)\right)v_n^2\}\end{aligned} \quad , \tag{B-13}$$

When substituting equations B-5, B-6, B-7 and B-8 into equations A-9 and A-10, we have

$$\tau_{R2}(x,z) = \tau_{R2F}(x,z)\tau_{R0}(x,z) - \tau_{I2F}(x,z)\tau_{I0}(x,z) \quad , \tag{B-14}$$

and

$$\tau_{I2}(x,z) = \tau_{R2F}(x,z)\tau_{I0}(x,z) + \tau_{I2F}(x,z)\tau_{R0}(x,z) \quad , \tag{B-15}$$

where

$$\tau_{R2F}(x,z) = \frac{\tau_{R2FU1}(x,z) + \tau_{R2FU2}(x,z) + \tau_{R2FU3}(x,z)}{\tau_{R2FD}(x,z)} \quad , \tag{B-16}$$

and

$$\tau_{I2F}(x,z) = \frac{\tau_{I2FU1}(x,z) + \tau_{I2FU2}(x,z) + \tau_{I2FU3}(x,z)}{\tau_{I2FD}(x,z)} \quad , \tag{B-17}$$

where

$$\tau_{R2FU1}=\frac{3}{2}\left\{-4v_0^{\,4}\left(b^6\sin^6\theta-15b^4\sin^4\theta X^2+15b^2\sin^2\theta X^4-X^6\right)\left(b^2\cos^2\theta+Z^2\right)^2 v_n+\left(b^2\sin^2\theta+X^2\right)^8 v_n^5\right\}\ ,$$

(B-18)

$$\begin{aligned}\tau_{R2FU2}=\frac{3}{2}\{&v_0^{\,2}\{4b^{16}\cos^2\theta\sin^{14}\theta+X^8\left(1+4X^6\right)Z^2+4b^{12}\sin^{10}\theta X^2\left(9\cos^2\theta X^2+24\cos\theta\sin\theta XZ-5\sin^2\theta Z^2\right)\\&+4b^{14}\sin^{12}\theta\left(5\cos^2\theta X^2+4\cos\theta\sin\theta XZ-\sin^2\theta Z^2\right)\\&-b^{10}\sin^8\theta\left[\cos^2\theta\left(1-20X^6\right)-240\cos\theta\sin\theta X^5Z+36\sin^2\theta X^4Z^2\right]\\&+b^8\sin^6\theta\left[-4\cos^2\theta X^2\left(-7+5X^6\right)+16\cos\theta\sin\theta X\left(-1+20X^6\right)Z+\sin^2\theta\left(1-20X^6\right)Z^2\right]\}\}\end{aligned}$$

, (B-19)

$$\begin{aligned}\tau_{R2FU3}=\frac{3}{2}\{&v_0^{\,2}\{2b^6\sin^4\theta X^2\left[-\cos^2\theta X^2\left(35+18X^6\right)+8\cos\theta\sin\theta X\left(7+15X^6\right)Z+2\sin^2\theta\left(-7+5X^6\right)Z^2\right]\\&+b^2X^6\left[-\cos^2\theta\left(X^2+4X^8\right)+16\cos\theta\sin\theta X\left(1+X^6\right)Z+4\sin^2\theta\left(-7+5X^6\right)Z^2\right]\\&+2b^4\sin^2\theta X^4\left[-2\cos^2\theta X^2\left(-7+5X^6\right)+8\cos\theta\sin\theta X\left(-7+6X^6\right)Z+\sin^2\theta\left(35+18X^6\right)Z^2\right]v_n^3\}\}\end{aligned}$$

, (B-20)

and

$$\begin{aligned}\tau_{R2FD}=&v_0^{\,4}\left(b^2\cos^2\theta+Z^2\right)^2+\left(b^2\sin^2\theta+X^2\right)^8 v_n^4\\&-2v_0^{\,2}v_n^2\{b^{10}\cos^2\theta\sin^8\theta-X^8Z^2-b^8\sin^6\theta\left(28\cos^2\theta X^2-16\cos\theta\sin\theta XZ+\sin^2\theta Z^2\right)\\&+14b^6\sin^4\theta X^2\left(5\cos^2\theta X^2-8\cos\theta\sin\theta XZ+2\sin^2\theta Z^2\right)-14b^4\sin^2\theta X^4\\&\left(2\cos^2\theta X^2-8\cos\theta\sin\theta XZ+5\sin^2\theta Z^2\right)+b^2X^6\left[\cos^2\theta X^2-16\cos\theta\sin\theta XZ+28\sin^2\theta Z^2\right]\}\end{aligned}$$

, (B-21)

and

$$\tau_{I2FU1}=3bv_0^{\,2}v_n\left\{4\sin\theta v_0^{\,2}X\left(3b^4\sin^4\theta-10b^2\sin^2\theta X^2+3X^4\right)\left(b^2\cos^2\theta+Z^2\right)^2\right\}.\quad\text{(B-22)}$$

$$\begin{aligned}\tau_{I2FU2}=3bv_0^{\,2}v_n\{&v_n^2\{4b^{14}\cos\theta\sin^{13}\theta\left(\cos\theta X-\sin\theta Z\right)+X^7Z\left[\cos\theta X\left(-1+4X^6\right)-4\sin\theta\left(-1+X^6\right)Z\right]\\&-4b^{12}\sin^{11}\theta X\left(-6\cos^2\theta X^2+5\cos\theta\sin\theta XZ+\sin^2\theta Z^2\right)\\&-12b^{10}\sin^9\theta X^3\left(-5\cos^2\theta X^2+3\cos\theta\sin\theta XZ+2\sin^2\theta Z^2\right)\\&-b^8\sin^7\theta\left[-4\cos^2\theta\left(X+20X^7\right)+\cos\theta\sin\theta\left(1+20X^6\right)Z+60\sin^2\theta X^5Z^2\right]\}\}\end{aligned}$$

. (B-23)

$$\tau_{I2FU3} = 3bv_0{}^2v_n\{v_n^2\{2b^4\sin^3\theta X^3\left[2\cos^2\theta X^2\left(7+6X^6\right)+\cos\theta\sin\theta X\left(-35+18X^6\right)Z+2\sin^2\theta\left(7-15X^6\right)Z^2\right]$$
$$+4b^2\sin\theta X^5\left[\cos^2\theta X^2\left(-1+X^6\right)+\cos\sin\theta X\left(7+5X^6\right)Z-\sin^2\theta\left(7+6X^6\right)Z^2\right]$$
$$+4b^6\sin^5\theta X\left[\cos^2\theta X^2\left(-7+15X^6\right)+\cos\theta\sin\theta X\left(7+5X^6\right)Z-\sin^2\theta\left(1+20X^6\right)Z^2\right]\}\}$$

. (B-24)

REFERENCES

Alkhalifah, T., 2000, An acoustic wave equation for anisotropic media: Geophysics, 65, 1239–1250.

Alkhalifah, T., 2011a, Scanning anisotropy parameters in complex media: Geophysics, 76, no. 2, U13–U22.

Alkhalifah, T., 2011b, Traveltime approximations for transversely isotropic media with an inhomogeneous background: Geophysics, 76, no. 3, WA31–WA42.

Alkhalifah, T., 2013, Traveltime approximations for inhomogeneous transversely isotropic media with a horizontal symmetry axis: Geophysical Prospecting, 61, 495–503.

Babich, V. M., and V. E. Nomofilov, 1981, Ray solutions with a complex eikonal concentrated in the vicinity of the geodesic: Russian Mathematical Surveys, 36, 198–212.

Bender, C. M., and S. A. Orszag, 1978, Advanced mathematical methods for scientists and engineers: McGraw-Hill.

Červený, V., 2001, Seismic ray theory: Cambridge university press.

Červený V., M. M. Popov, and I. Pšenčík, 1982, Computation of wave fields in inhomogeneous media—Gaussian beam approach: Geophysical Journal International, 70, 109–128.

Chapman, S. J., J. M. Lawry, J. R. Ockendon, and R. H. Tew, 1999, On the theory of complex rays: SIAM review, 41, 417–509.

Choudhary, S., and L. B. Felsen, 1974, Analysis of Gaussian beam propagation and diffraction by inhomogeneous wave tracking: Proceedings of the IEEE, 62, 1530–1541.

da Silva, N. V., A. Ratcliffe, V. Vinje, and G. Conroy, 2016, A new parameter set for anisotropic multiparameter full-waveform inversion and application to a North Sea data set: Geophysics, 81, no. 4, U25–U38.

Deschamps, G. A., 1971, Gaussian beam as a bundle of complex rays: Electronics letters, 7, 684–685.

Duveneck, E., and P. Bakker, 2011, Stable P-wave modeling for reverse-time migration in tilted TI media: Geophysics, 76, no. 2, S65–S75.

Egorchenkov, R. A., and Y. A. Kravtsov, 2001, Complex ray-tracing algorithms with application to optical problems: Journal of the Optical Society of America A, 18, 650–656.

Felsen, L. B., 1976, Evanescent waves: Journal of the Optical Society of America, 66, 751–760.

Felsen, L. B., 1984, Geometrical theory of diffraction, evanescent waves, complex rays and Gaussian beams: Geophysical Journal International, 79, 77–88.

Golikov, P., and A. Stovas, 2012, Traveltime parameters in a tilted elliptical anisotropic medium: Geophysical Prospecting, 60, 433–443.

Gray, S. H., 2005, Gaussian beam migration of common-shot records: Geophysics, 70, no. 4, S71–S77.

Gray, S. H., and N. Bleistein, 2009, True-amplitude Gaussian-beam migration: Geophysics, 74, no. 2, S11–S23.

Grechka, V., L. Zhang, and J. W. Rector, 2004, Shear waves in acoustic anisotropic media: Geophysics, 69, 576–582.

Hao Q., A. Stovas, and T. Alkhalifah, 2016, The offset-midpoint traveltime pyramid of P-waves in homogeneous orthorhombic media: Geophysics, 81, no. 5, C151–C162.

Hao, Q., and T. Alkhalifah, 2017a, An acoustic eikonal equation for attenuating transversely isotropic media with a vertical symmetry axis: Geophysics, 82, no. 1, C9–C20.

Hao, Q., and T. Alkhalifah, 2017b, An acoustic eikonal equation for attenuating orthorhombic media: Geophysics, 82, no. 4, WA67–WA81.

Hao, Q., U. Waheed, and T. Alkhalifah, 2018, A Fast Sweeping Scheme for P-wave Traveltimess in Attenuating VTI Media: 80th EAGE Conference and Exhibition.

Hearn, D. J., and S. E. Krebes, 1990a, On computing ray-synthetic seismograms for anelastic media using complex rays: Geophysics, 55, 422–432.

Hearn, D. J., and E. S. Krebes, 1990b, Complex rays applied to wave propagation in a viscoelastic medium: Pure and Applied Geophysics, 132, 401–415.

Hill, N. R., 1990, Gaussian beam migration: Geophysics, 55, 1416–1428.

Hill, N. R., 2001, Prestack Gaussian-beam depth migration: Geophysics, 66, 1240–1250.

Huang, X., 2018, Extended beam approximation for high-frequency wave propagation: *IEEE Access*, *6*, 37214–37224.

Huang X, H. Sun, and J. Sun, 2016a, Born modeling for heterogeneous media using the Gaussian beam summation based Green's function: Journal of Applied Geophysics, 131, 191–201.

Huang, X., J. Sun, and Z. Sun, 2016b, Local algorithm for computing complex travel time based on the complex eikonal equation: Physical Review E, 93, 043307.

Huang X., and S. Greenhalgh, 2018, Linearized formulations and approximate solutions for the complex eikonal equation in orthorhombic media and applications of complex seismic traveltime: Geophysics, 83, no. 3, C115–C136.

Huang X., J. Sun, and S. Greenhalgh, 2018, On the solution of the complex eikonal equation in acoustic VTI media: A perturbation plus optimization scheme: Geophysical Journal International, *214*, 907–932.

Huang, X., M. Jakobsen, G. Naevdal, and K. S. Eikrem, 2019, Target-Oriented Inversion of Time-Lapse Seismic Waveform Data: Communications in Computational Physics, doi: 10.4208/cicp.OA-2018-0143.

Huang, X., and S. Greenhalgh, 2019, Traveltime approximation for strongly anisotropic media using the homotopy analysis method: Geophysical Journal International, 216 , 1648–1664.

Ivanov, Y., and A. Stovas, 2019, 3D mapping of kinematic attributes in anisotropic media: Geophysics, 84, no. 3, C159–C170.

Klimeš, M., and L. Klimeš, 2011, Perturbation expansions of complex-valued traveltime along real-valued reference rays: Geophysical Journal International, 186, 751–759.

Kravtsov, Y. A., G. W. Forbes, and A. A. Asatryan, 1990, Theory and applications of complex rays: Progress in optics, 39, 1–62.

Krebes, E. S., and L. H. Le, 1994, Inhomogeneous plane waves and cylindrical waves in anisotropic anelastic media: Journal of Geophysical Research: Solid Earth, 99, 23899–23919.

Li, S., S. Fomel, and A. Vladimirsky, 2011, Improving wave-equation fidelity of Gaussian beams by solving the complex eikonal equation: SEG Technical Program Expanded Abstracts 2011, Society of Exploration Geophysicists, 3829–3834.

Magnanini, R., and G. Talenti , 1999, On complex-valued solutions to a 2D eikonal equation. Part one: qualitative properties: Contemporary Math, 283, 203–229.

Magnanini, R., and G. Talenti, 2003, On complex-valued solutions to a two-dimensional eikonal equation. II. Existence theorems: SIAM journal on mathematical analysis, 34, 805–835.

Magnanini, R., and G. Talenti, 2006, On complex-valued solutions to a 2D eikonal equation. Part Three: analysis of a Bäcklund transformation: Applicable Analysis, 85, 249–276.

Nomofilov, V. E., 1982, Asymptotic solutions of a system of equations of second order which are concentrated in a neighborhood of a ray: Journal of Soviet Mathematics, 20, 1854–1860.

Stovas, A., and T. Alkhalifah, 2012, A new traveltime approximation for TI media: Geophysics, 77, no. 4, C37–C42.

Terng, C. L., and U. Karen, 2000, Geometry of solitons: Notices of AMS, 47, 17–25.

Popov, M. M., 1982, A new method of computation of wave fields using Gaussian beams: Wave motion, 4, 85–97.

Thomsen, L., 1986, Weak elastic anisotropy: Geophysics, 51, 1954–1966.

Thomson, C. J., 1997, Complex rays and wave packets for decaying signals in inhomogeneous, anisotropic and anelastic media: Studia Geophysica et Geodaetica, 41, 345–381.

Vavryčuk, V., 2008a, Real ray tracing in anisotropic viscoelastic media: Geophysical Journal International, 175, 617–626.

Vavryčuk, V., 2008b, Velocity, attenuation, and quality factor in anisotropic viscoelastic media: A perturbation approach: Geophysics, 73, no. 5, D63–D73.

Vavryčuk, V., 2010, Behaviour of rays at interfaces in anisotropic viscoelastic media: Geophysical Journal International, 181, 1665–1677.

Vavryčuk, V., 2012, On numerically solving the complex eikonal equation using real ray-tracing methods: A comparison with the exact analytical solution: Geophysics, 77, no. 4, T109–T116.

Waheed, U. B., T. Alkhalifah, and A. Stovas , 2013, Diffraction traveltime approximation for TI media with an inhomogeneous background: Geophysics, 78, no. 5, WC103–WC111.

Wang, W. Y. D., and A. G. Deschamps,1974, Application of complex ray tracing to scattering problems: Proceedings of the IEEE, 62, 1541–1551.

Wu, R. S., 1985, Gaussian beams, complex rays, and the analytic extension of the Green's function in smoothly inhomogeneous media: Geophysical Journal International, 83, 93–110.

Zhang, Y., H. Zhang, and G. Zhang, 2011, A stable TTI reverse time migration and its implementation: Geophysics, 76, no. 3, WA3–WA11.

Zhu, T., and K. Y. Chun, 1994, Complex rays in elastic and anelastic media: Geophysical Journal International, 119, 269–279.

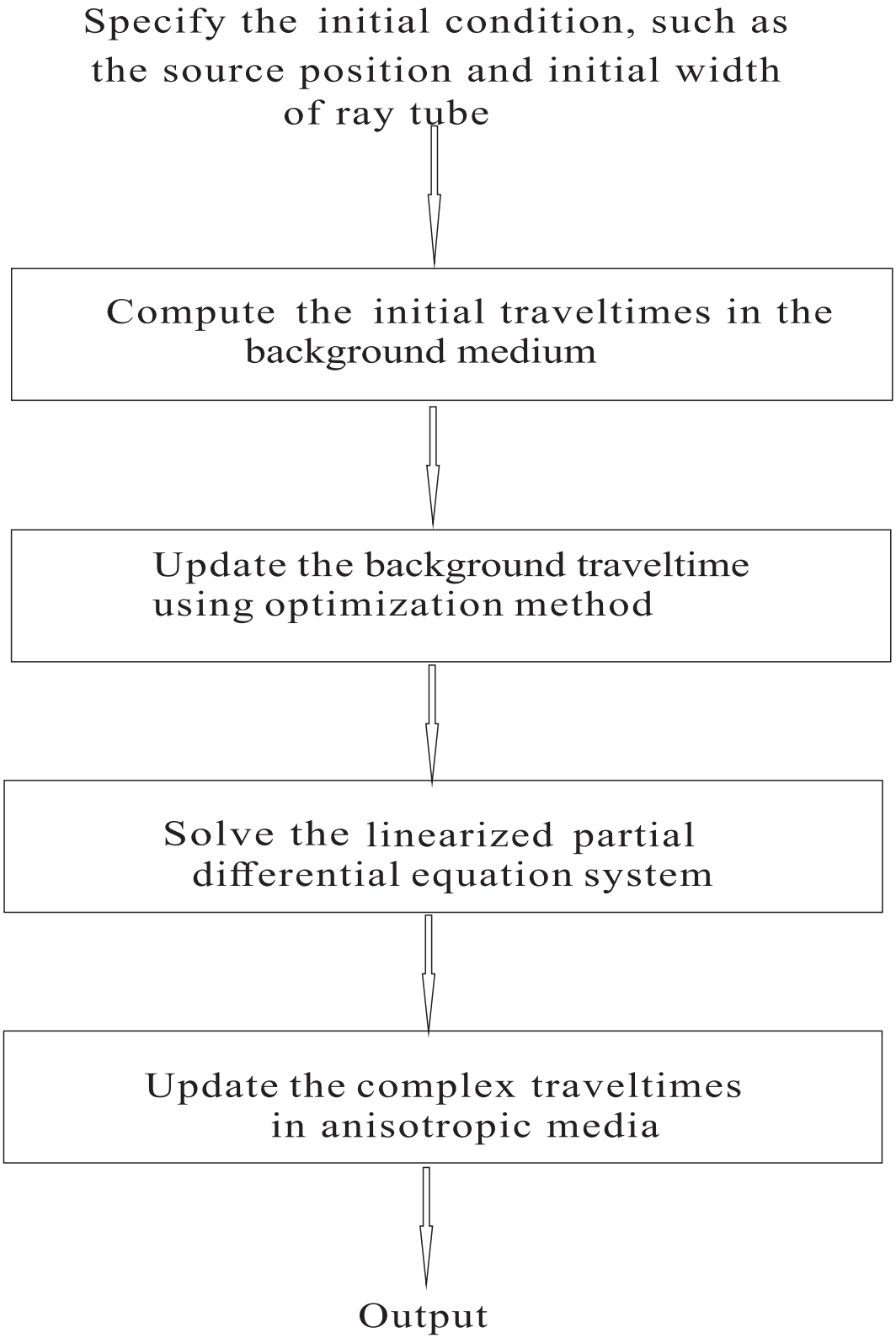

Figure 1. Schematic diagram for complex traveltime computation.

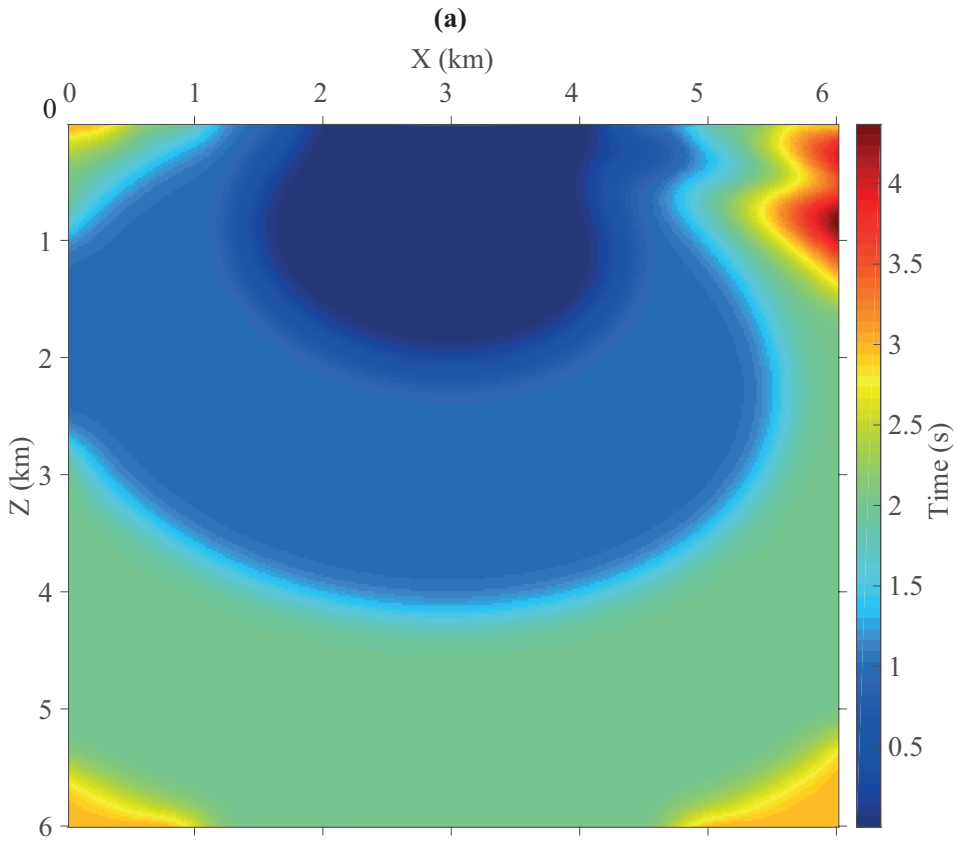
(a)
X (km)
0
1
2
3
4
5
6
Z (km)
0
1
2
3
4
5
6
Time (s)
4
3.5
3
2.5
2
1.5
1
0.5

(b)

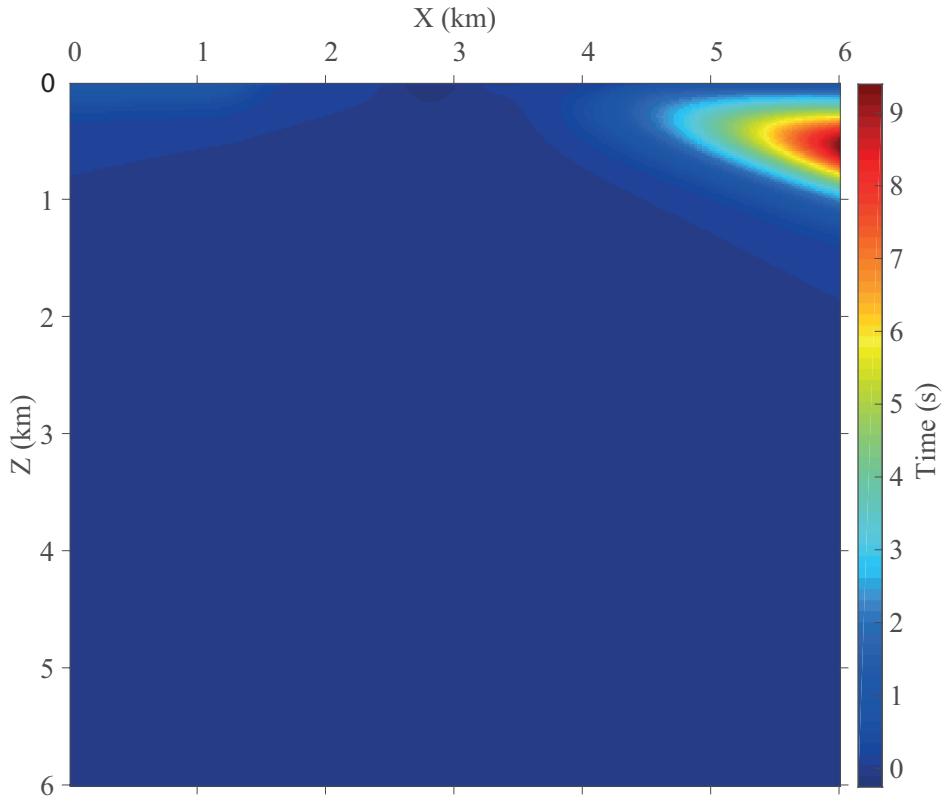

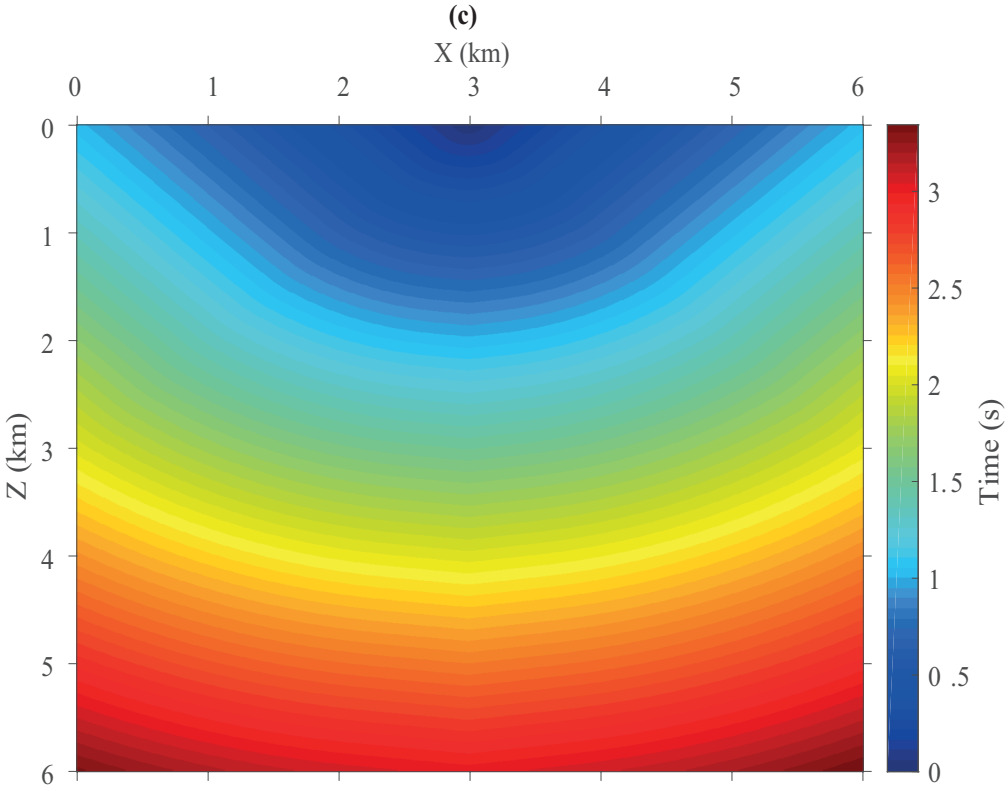
(c)
X (km)
0
1
2
3
4
5
6
Z (km)
0
1
2
3
4
5
6
Time (s)
3
2.5
2
1.5
1
0 .5
0

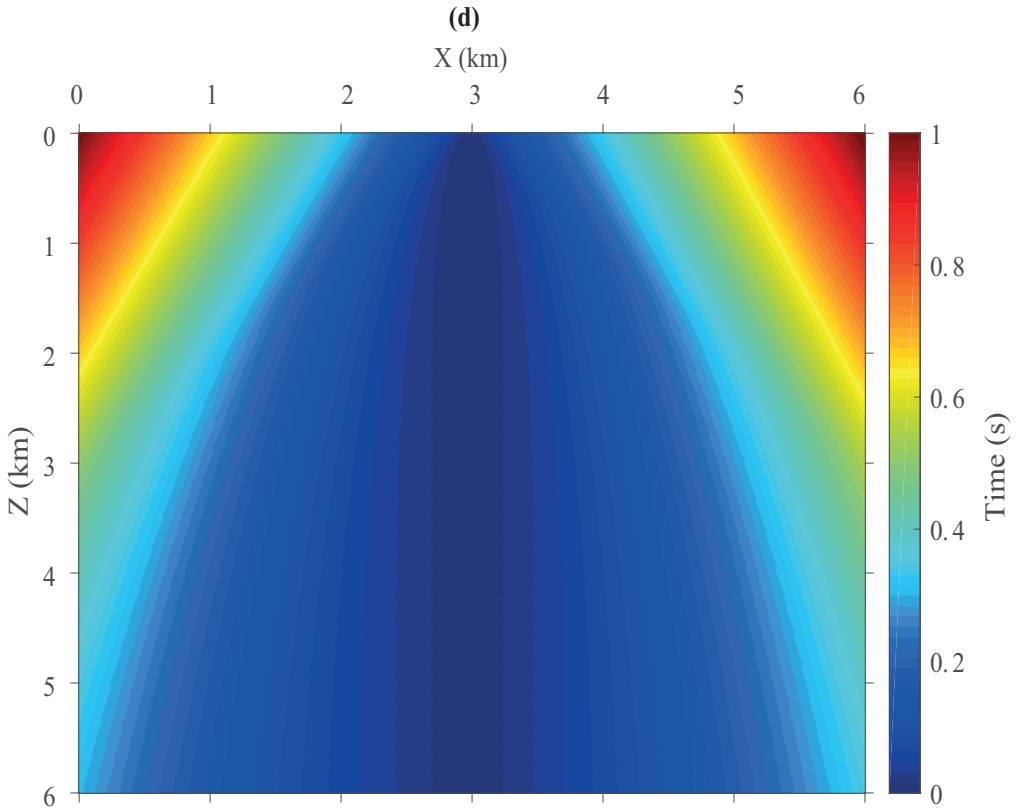

Figure 2. Plot of the complex traveltimes of a vertical beam for a TTI medium. All models have the same velocity $v_0 = 2\,\mathrm{km/s}$, $\theta = 10^0$, η=0.1 and $\delta = 0.05$. The starting point of the ray is at (3km, 0km), and the initial ray tube width is 200 m. Figures (a) and (b) show the real and imaginary parts of the complex traveltimes with the proposed method. Figures (c) and (d) show the real and imaginary parts of the complex traveltimes with dynamic ray tracing. The TTI medium for Figure (a) and (b) has $\eta = 0.1$.

(a)

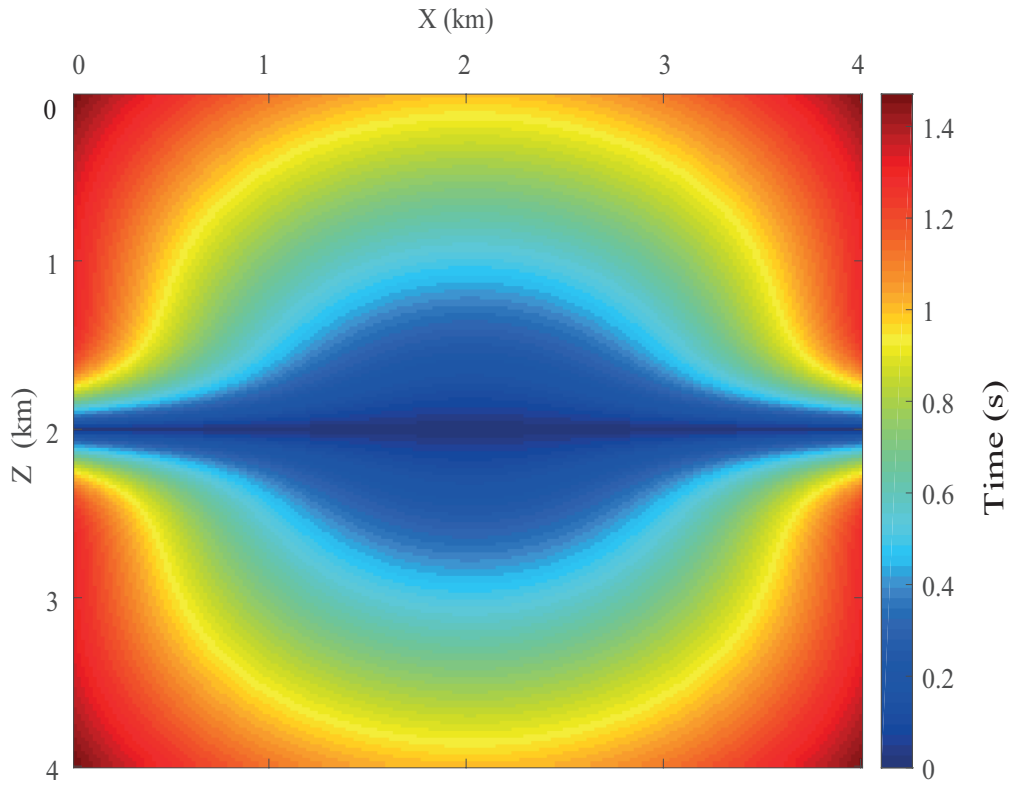

(b)

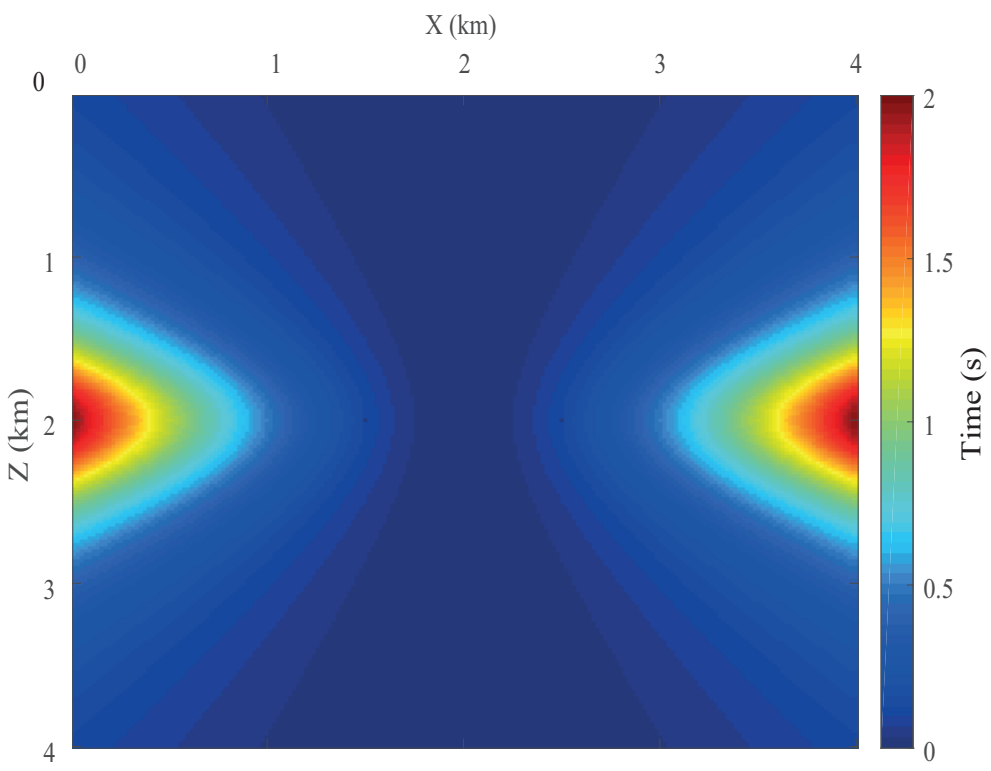

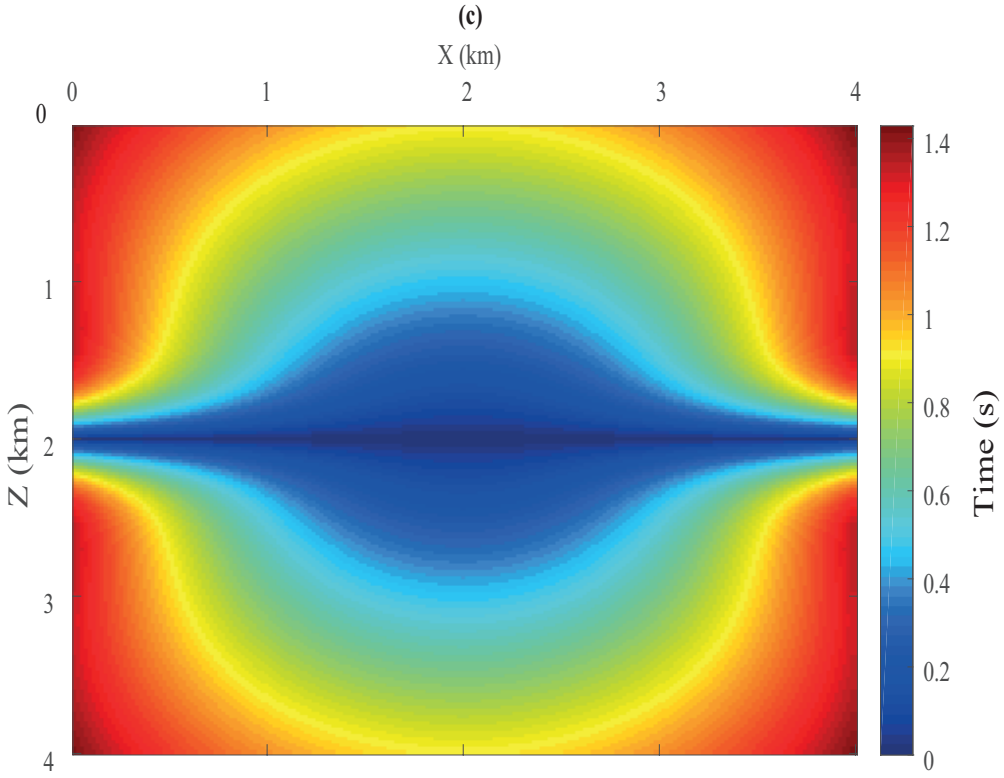
(c)
X (km)
0
1
2
3
4
Z (km)
0
1
2
3
4
Time (s)
1.4
1.2
1
0.8
0.6
0.4
0.2
0

(d)

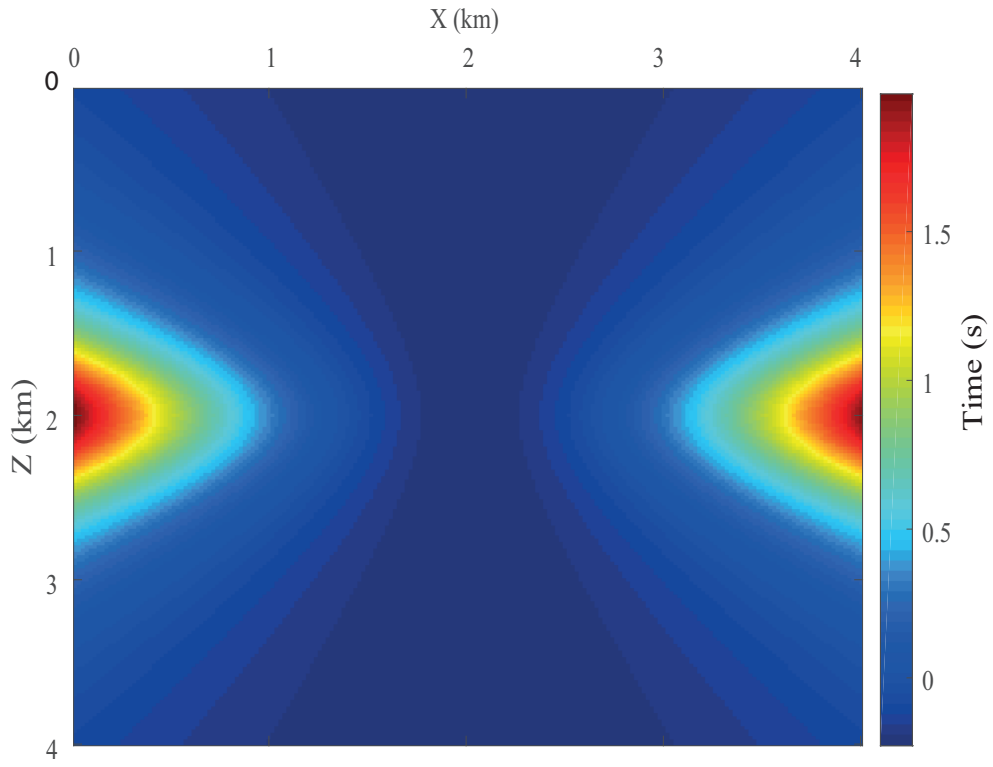

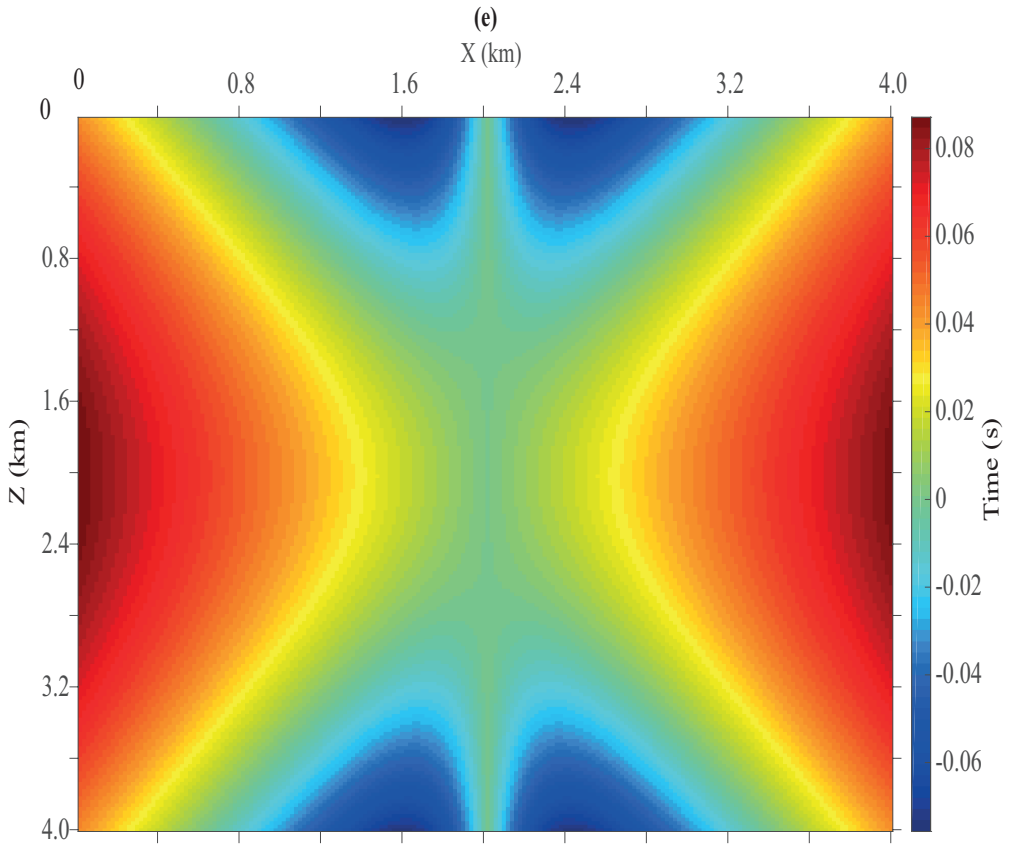
(e)
X (km)
0
0.8
1.6
2.4
3.2
4.0
Z (km)
0
0.8
1.6
2.4
3.2
4.0
0.08
0.06
0.04
0.02
0
-0.02
-0.04
-0.06
Time (s)

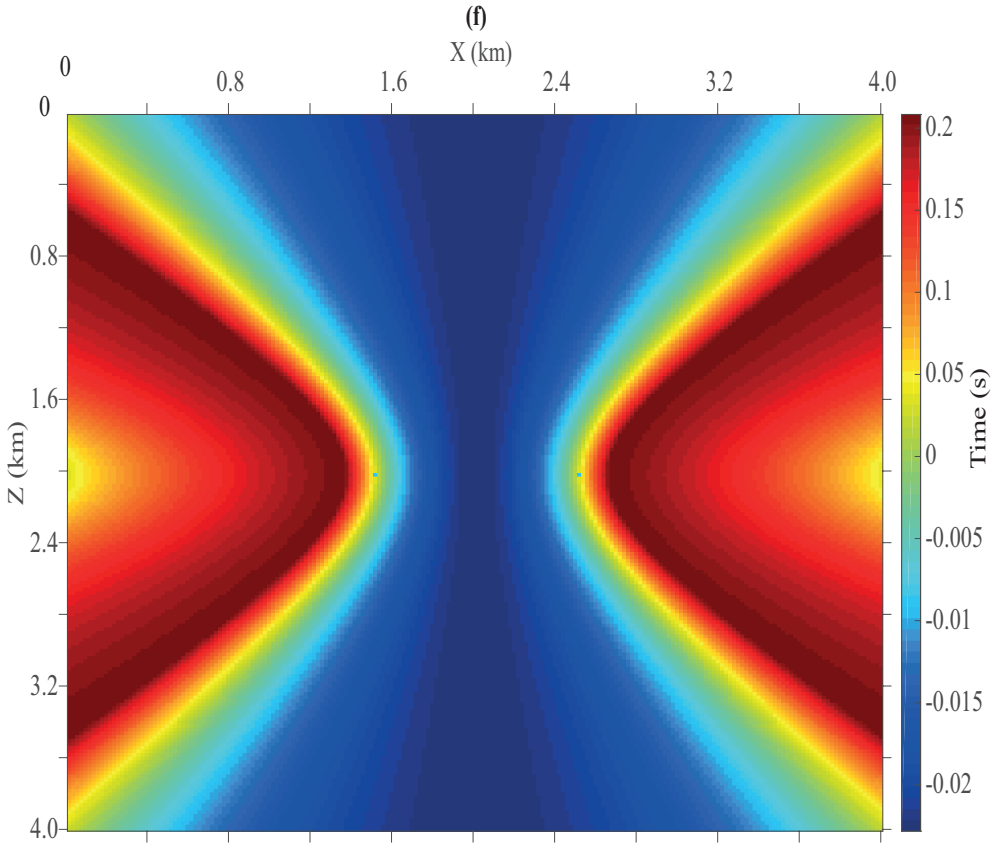

Figure 3. Comparison of complex traveltimes of a vertical beam with exact solutions. The starting point of the ray is at (2 km, 2 km), and the initial ray tube width is 500m. Figures (a) and (c) show the real part of the complex traveltimes, while Figures (b) and (d) show the imaginary part of the complex traveltimes. Figures (e) and (f) show the error of the real and imaginary parts, respectively.

(a)

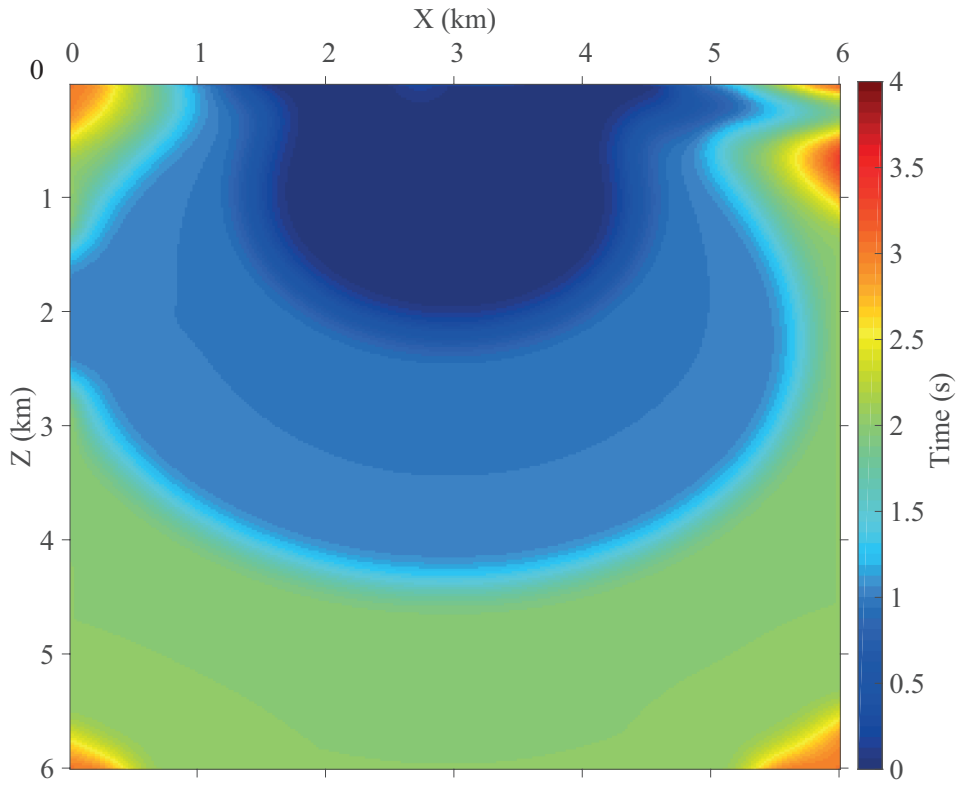

(b)

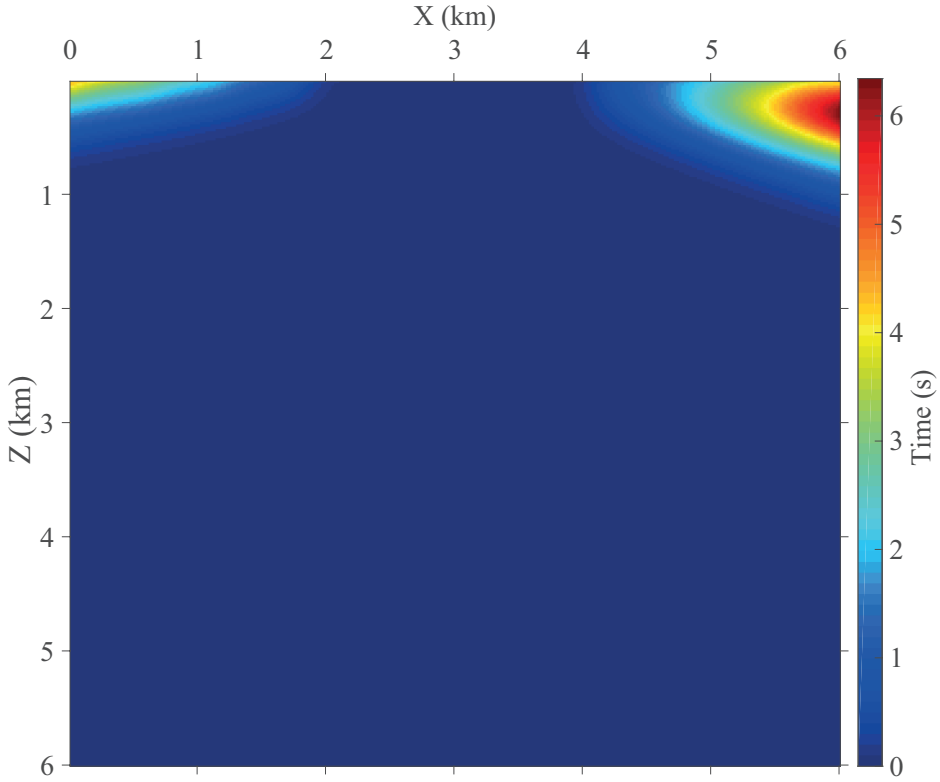

(c)

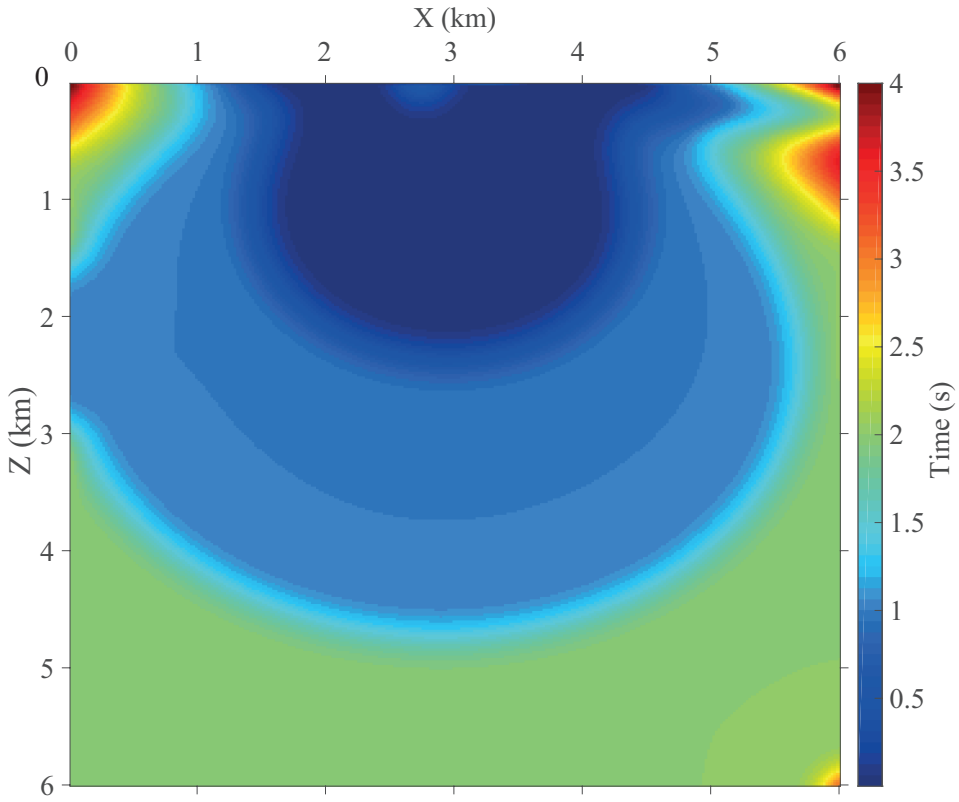

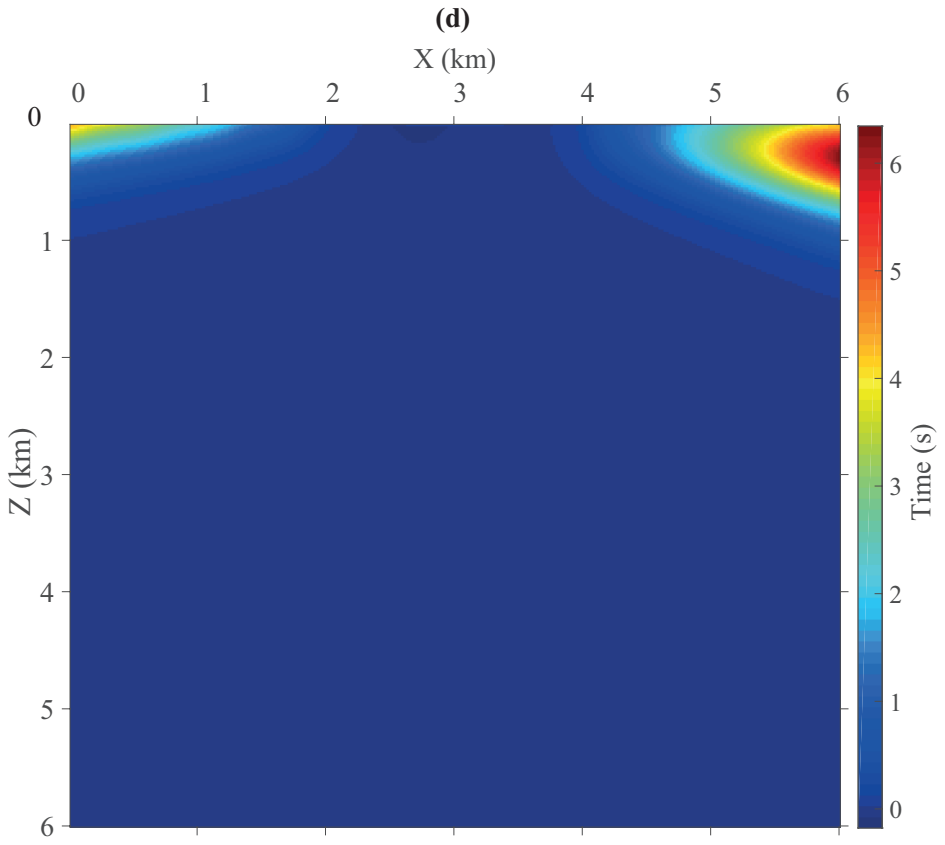

Figure 4. The complex traveltimes of a vertical beam for a TTI medium. The starting point of the ray is at (3 km, 0 km), and the initial ray tube width is 300 m. Figures (a) and (c) show the real part of the complex traveltimes, while Figures (b) and (d) show the imaginary part of the complex traveltimes. The TTI medium for Figures (a) and (b) has: $\eta = 0.05$ and for Figures (c) and (d): $\eta = 0.05$.

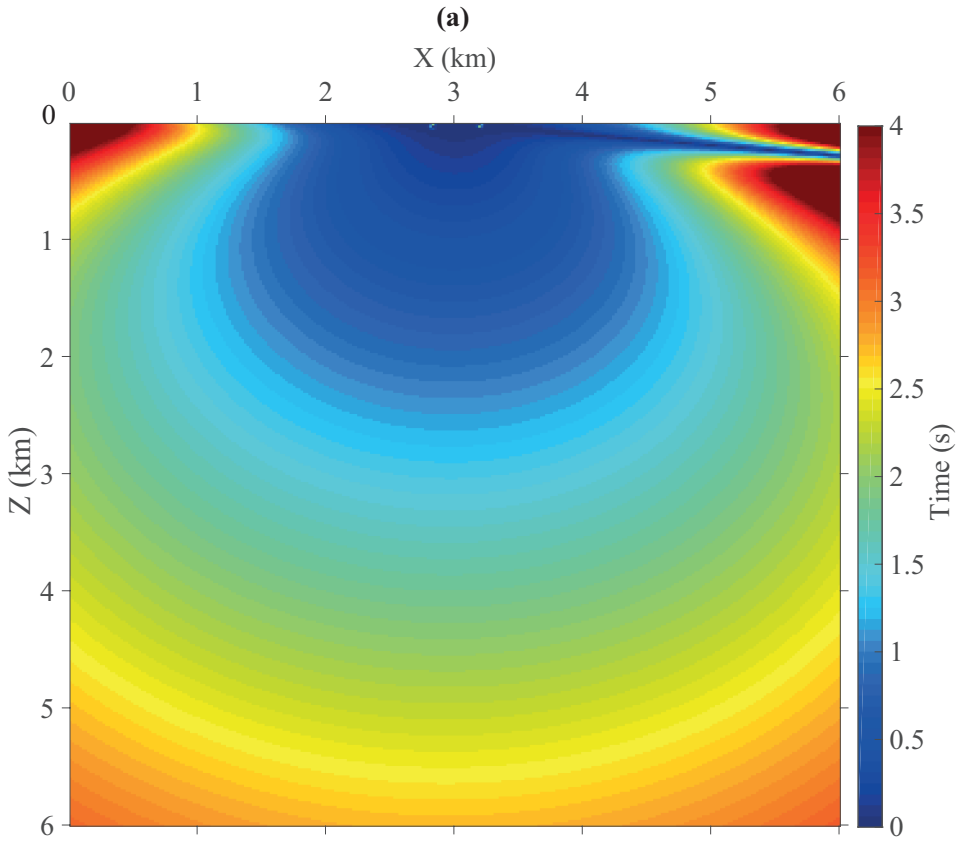
(a)
X (km)
0
1
2
3
4
5
6
Z (km)
0
1
2
3
4
5
6
Time (s)
4
3.5
3
2.5
2
1.5
1
0.5
0

(b)

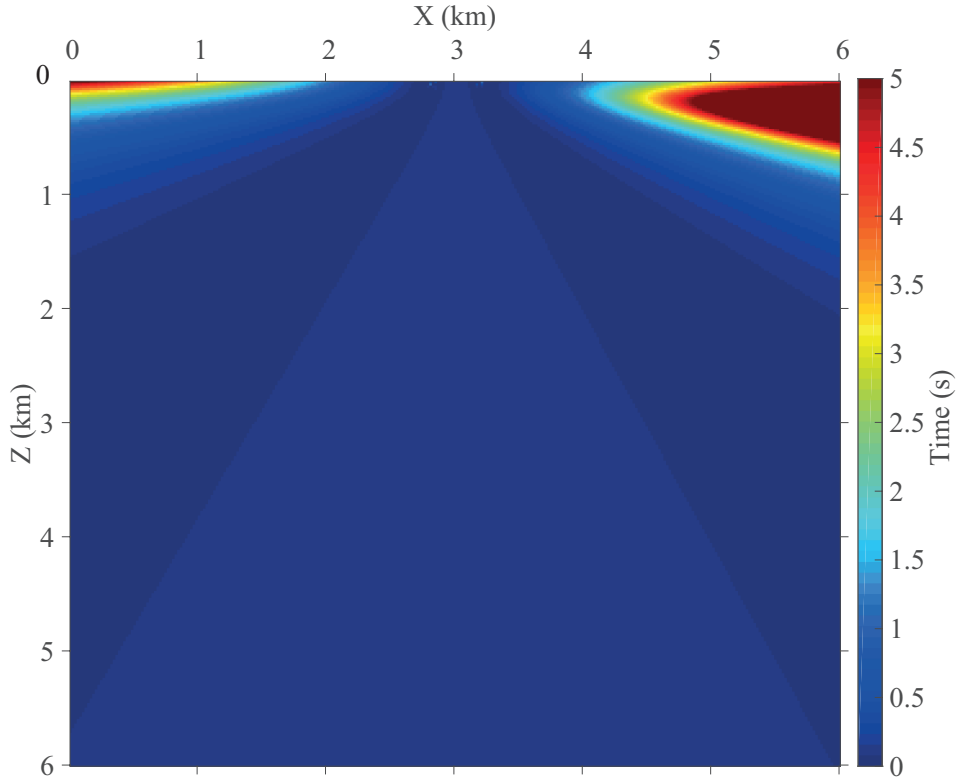
X (km)
0
1
2
3
4
5
6
Z (km)
0
1
2
3
4
5
6
Time (s)
5
4.5
4
3.5
3
2.5
2
1.5
1
0.5
0

(c)

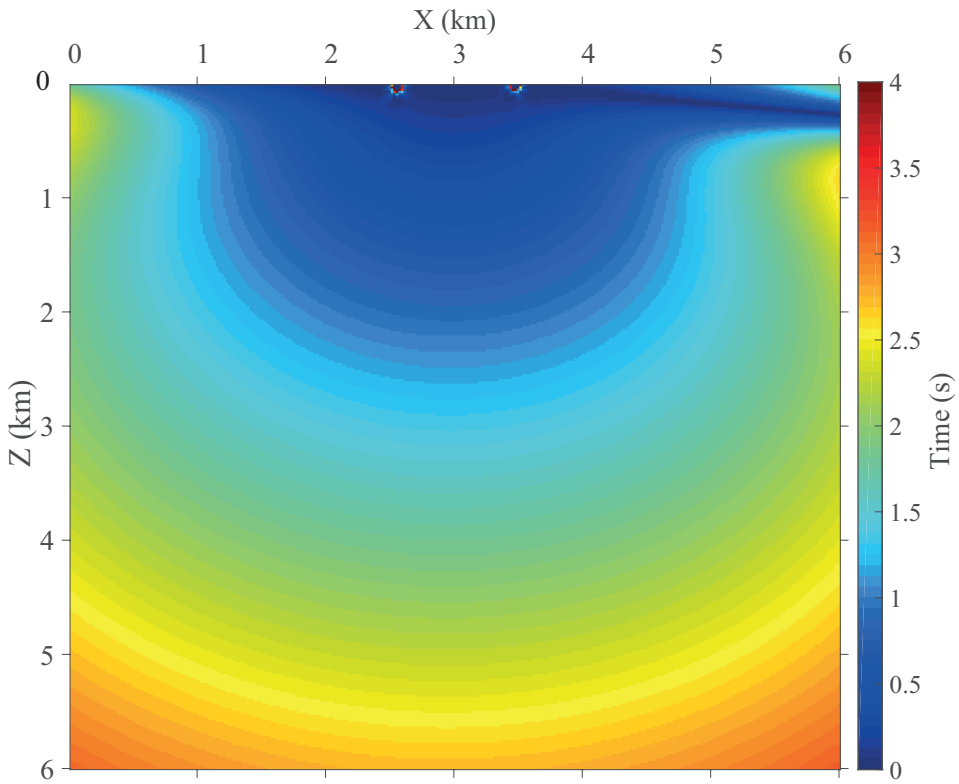
X (km)
0
1
2
3
4
5
6
Z (km)
0
1
2
3
4
5
6
Time (s)
4
3.5
3
2.5
2
1.5
1
0.5
0

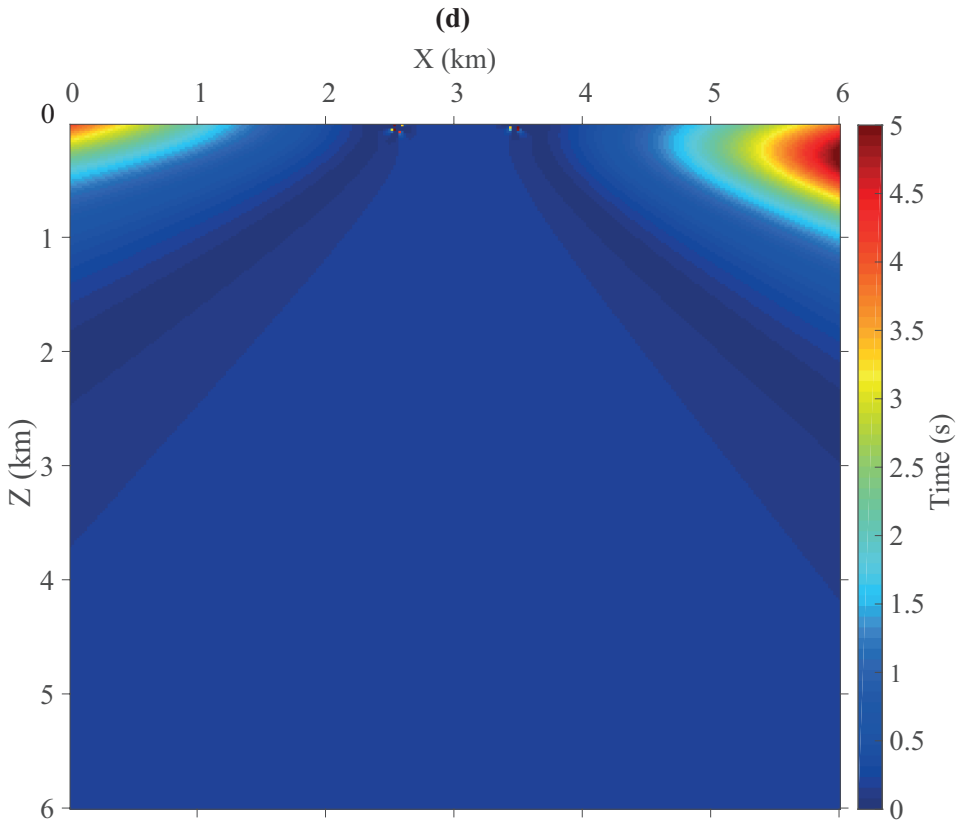

Figure 5. Plot of the complex traveltimes of a vertical beam for a TTI medium. The size of the model is $6\,\mathrm{km}\times 6\,\mathrm{km}$. The model velocity is $v_0 = 2$ km/s, and the anisotropic parameters are $\eta = 0.1$, $\delta = 0.1$ and $\theta = 5^0$, respectively. The starting point of the ray is at (3 km, 0 km), and $\eta = 0.1$. Figures Figures (a) and (c) show the real part of the complex traveltimes, while Figures (b) and (d) show the imaginary part of the complex traveltimes. The initial ray tube width for Figures (a) and (b) is 200 m. The initial ray tube width for (c) and (d) is 500 m.

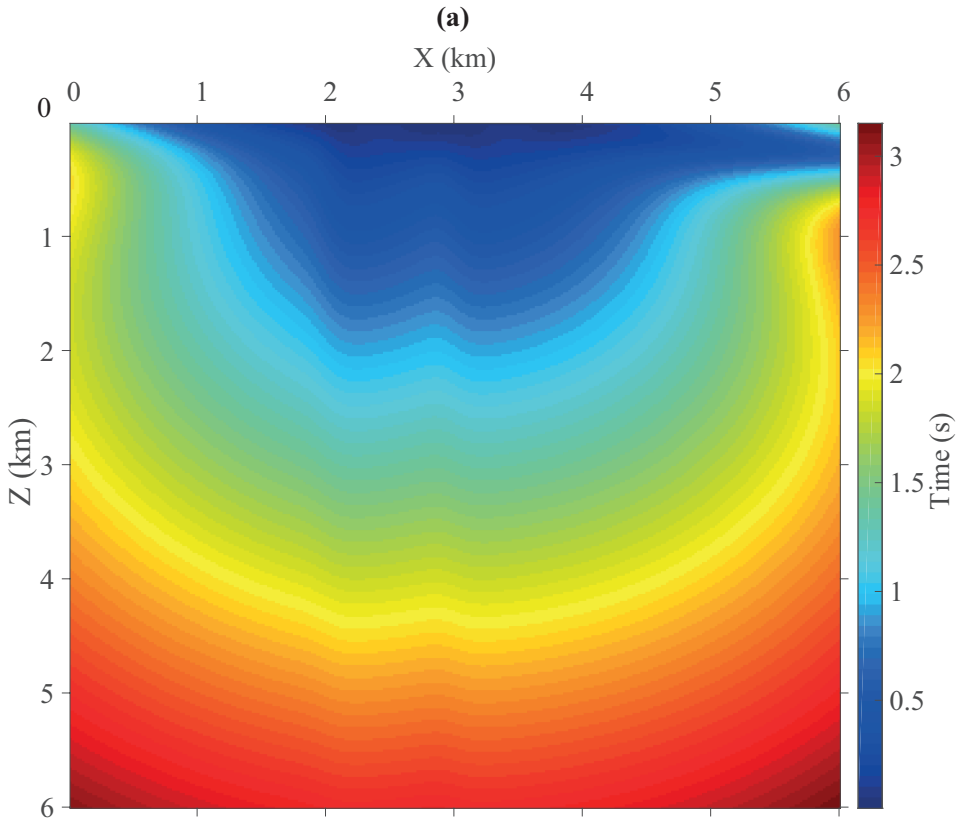
(a)
X (km)
0
1
2
3
4
5
6
Z (km)
0
1
2
3
4
5
6
Time (s)
3
2.5
2
1.5
1
0.5

(b)

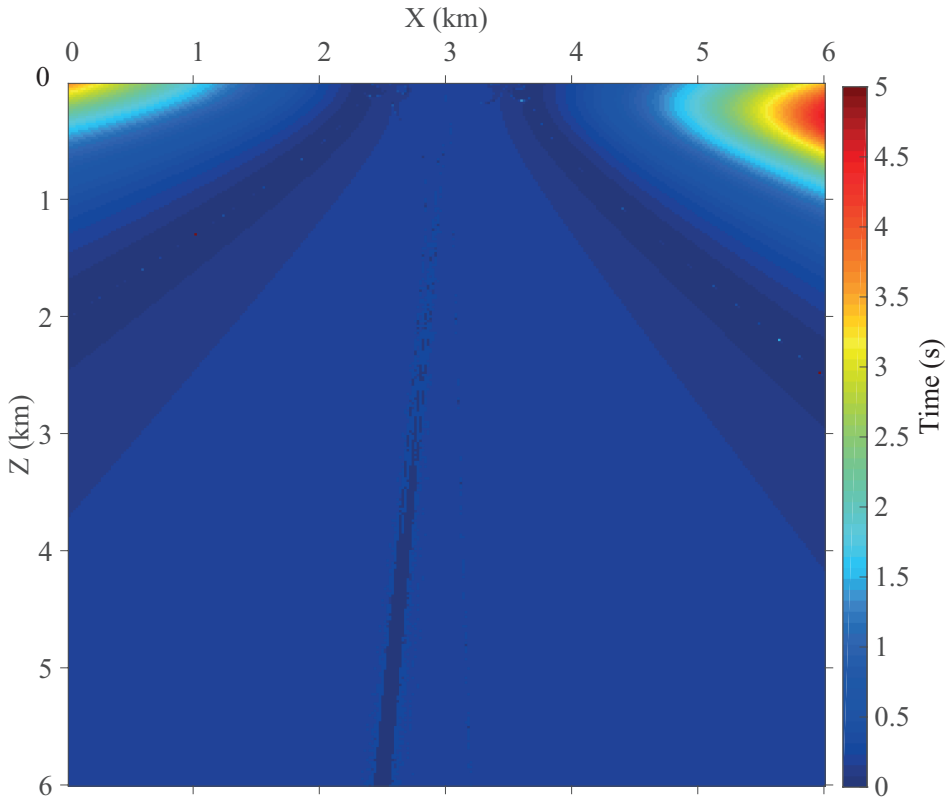

(c)

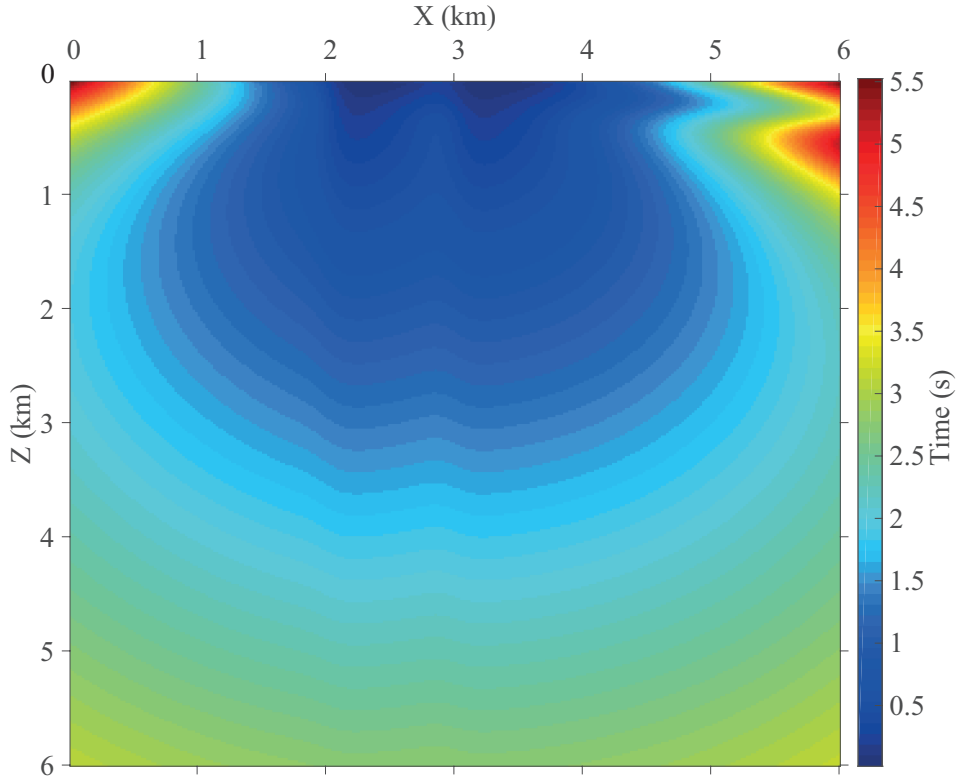
X (km)
0
1
2
3
4
5
6
Z (km)
0
1
2
3
4
5
6
Time (s)
5.5
5
4.5
4
3.5
3
2.5
2
1.5
1
0.5

(d)

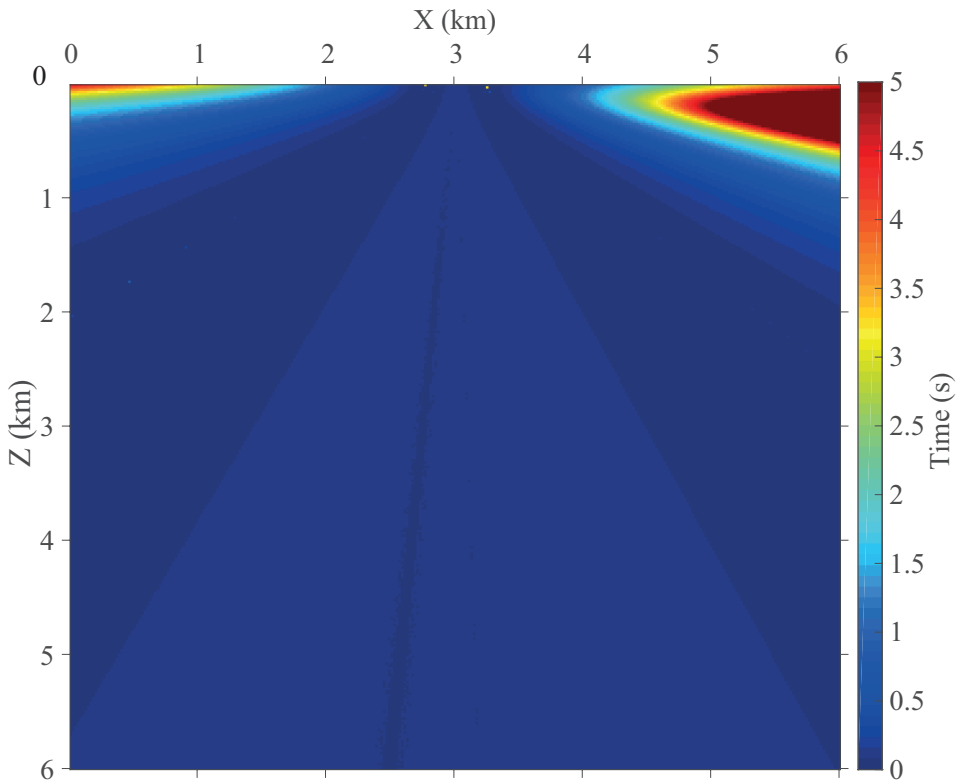
X (km)
0
1
2
3
4
5
6
Z (km)
0
1
2
3
4
5
6
Time (s)
5
4.5
4
3.5
3
2.5
2
1.5
1
0.5
0

Figure 6. The complex traveltimes of a vertical beam for a TTI medium using the Shanks transform. The size of the model is $6\,\mathrm{km}\times 6\,\mathrm{km}$. The model velocity is $v_0 = 2\,\mathrm{km/s}$, and the anisotropic parameters are $\eta = 0.1$, $\delta = 0.1$ and $\theta = 5^0$, respectively. The starting point of the ray is at (3 km, 0 km), and $\eta = 0.1$. Figures (a) and (c) show the real part of the complex traveltimes, while Figures (b) and (d) show the imaginary part of the complex traveltimes. The initial of ray tube width for Figures (a) and (b) is 500 m. The initial ray tube width for Figures (c) and (d) is 200. m.

(a)

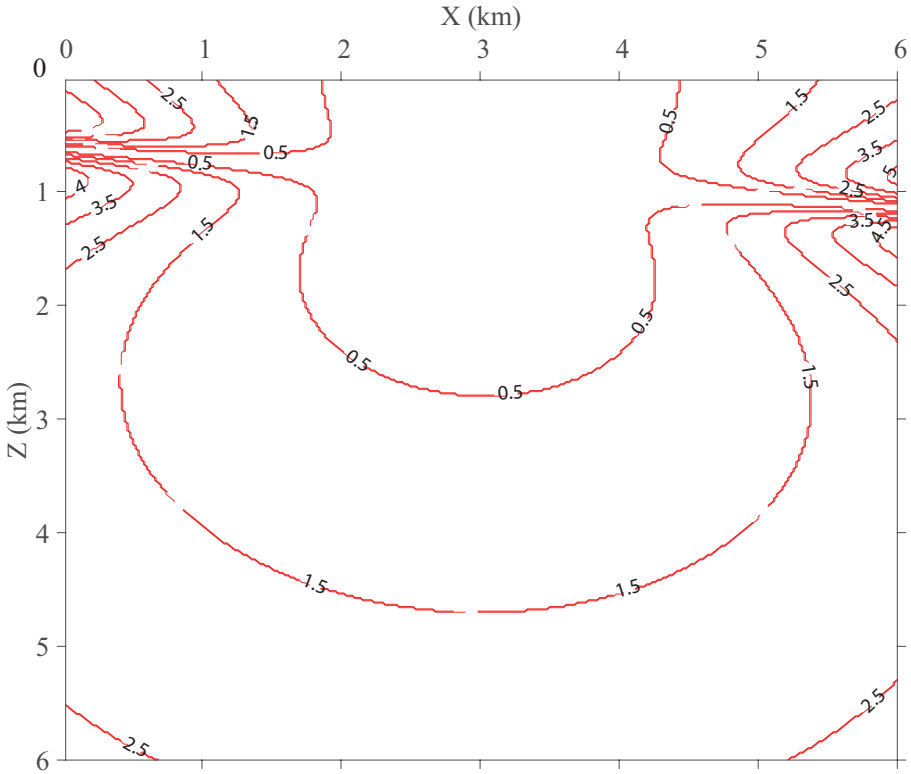

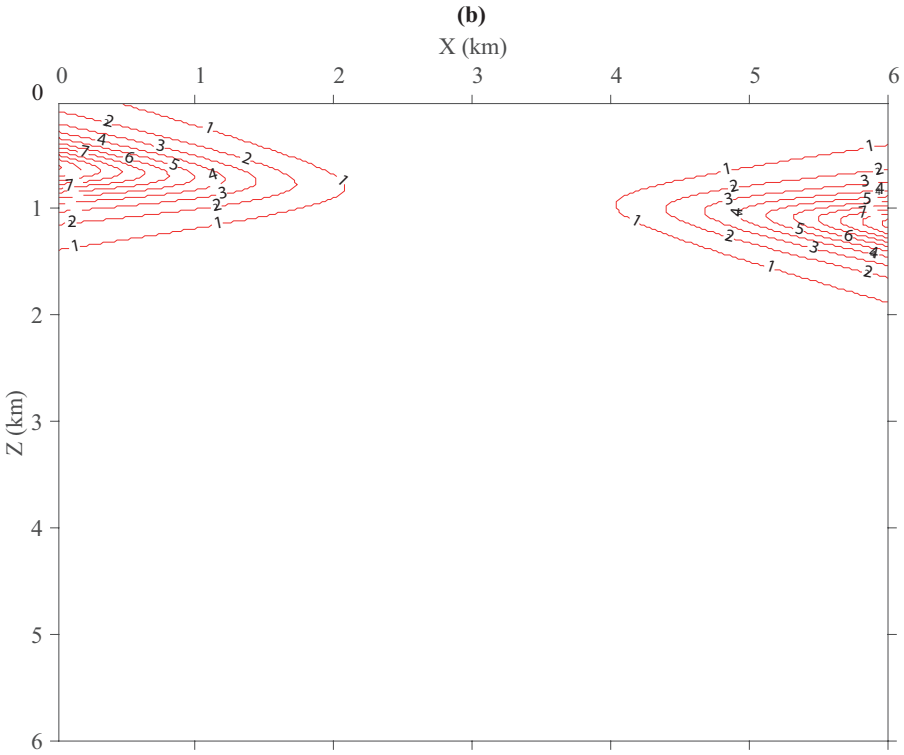
(b)
X (km)
0
1
2
3
4
5
6
Z (km)

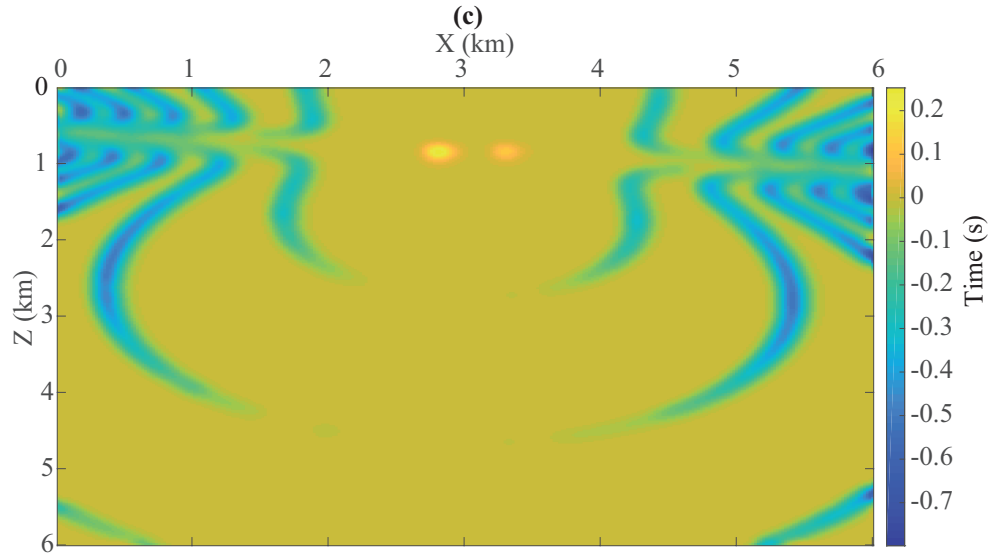
(c)
X (km)
0
1
2
3
4
5
6
Z (km)
0.2
0.1
0
-0.1
-0.2
-0.3
-0.4
-0.5
-0.6
-0.7
Time (s)

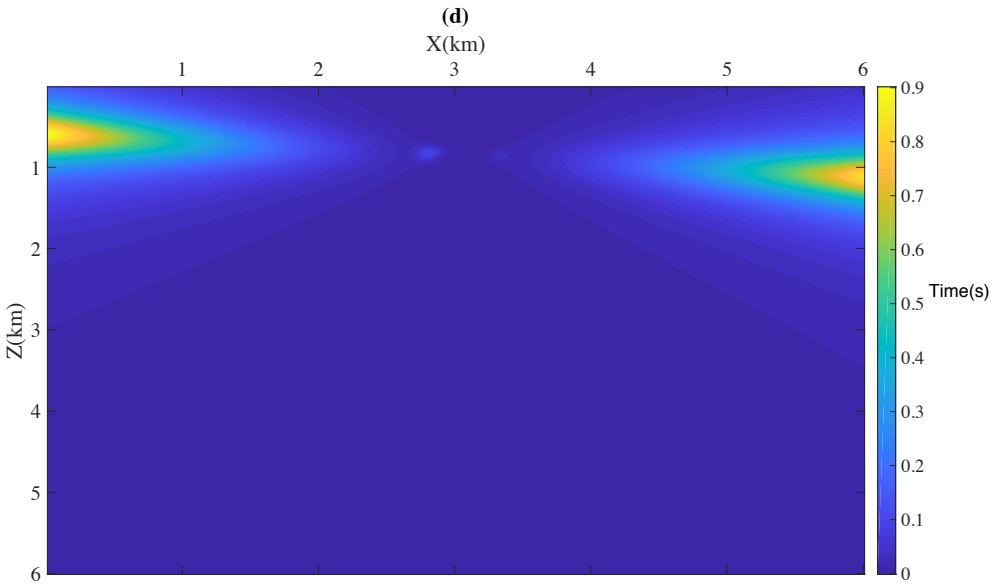

Figure 7. Comparison of the results for the TTI medium (green line) with those for the elliptically isotropic (red line) medium. The size of the model is $6\ \mathrm{km} \times 6\ \mathrm{km}$.. The model velocity is $v_0 = 2\ \mathrm{km/s}$. The starting point of the ray is at (3.5 km, 1 km), and $\eta = 0.1$ $\theta = 5^0$. The initial ray tube width is 300 m. Figure (a) the real part of the complex traveltimes, and Figure (b) the imaginary part of the complex traveltimes. Figures (c) and (d) show the time differences between the TTI medium and the elliptically isotropic medium.

(a)

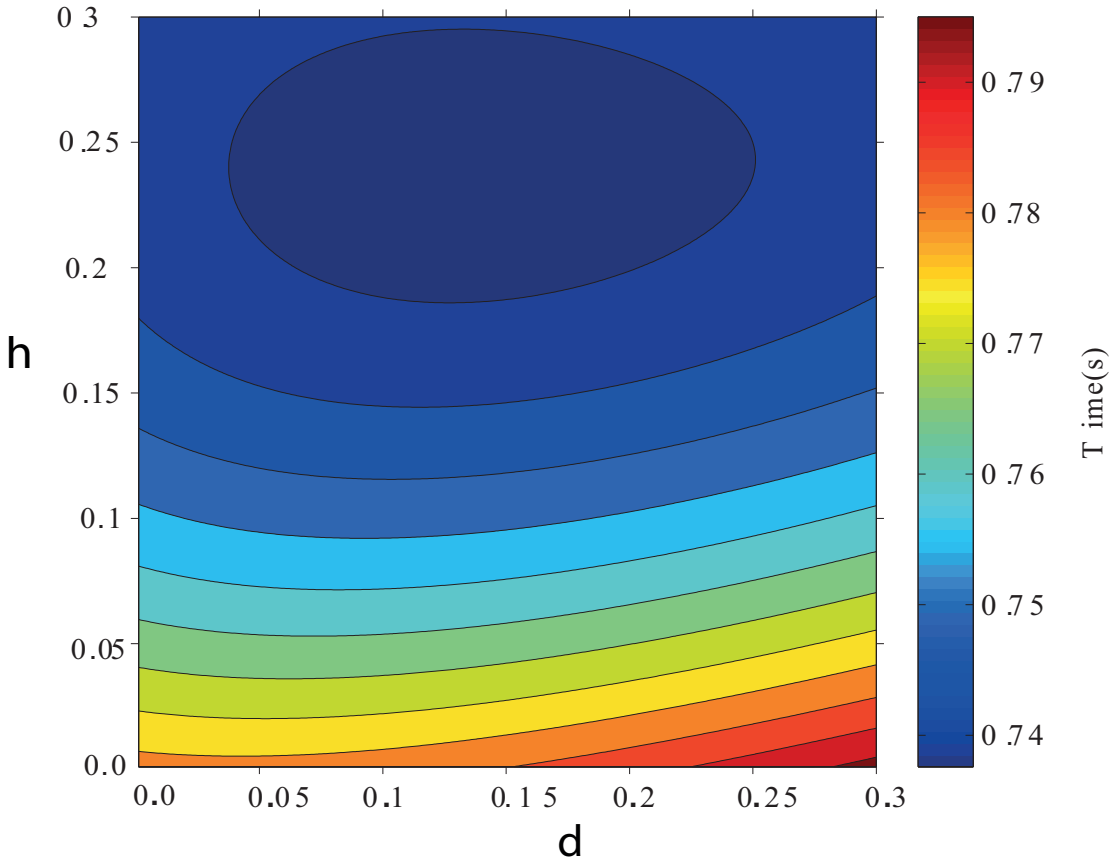
0 3
0 .25
0.2
0.15
0.1
0.05
0.0
h
0.0
0.05
0.1
0. 1 5
0.2
0.25
0.3
d
0 .79
0 .78
0 .77
0 .76
0 .75
0 .74
T ime(s)

(b)

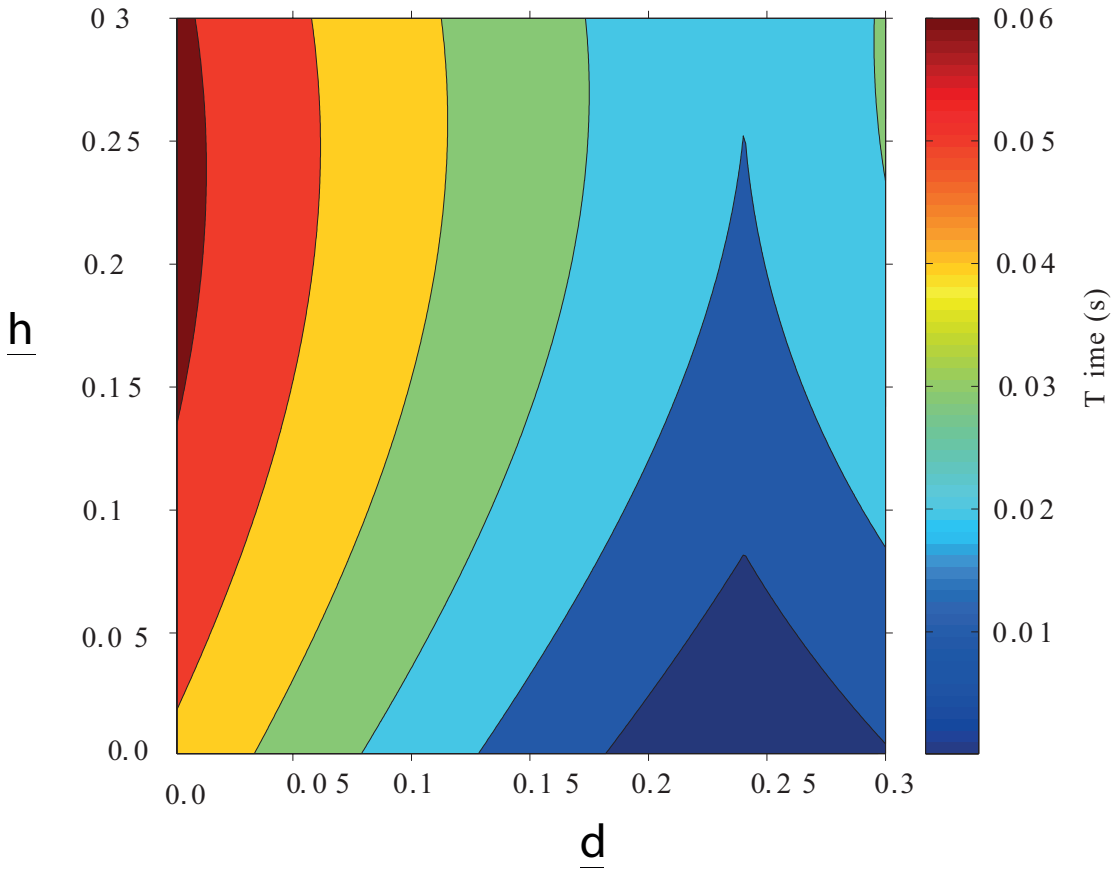
0 3
0.25
0.2
0.15
0.1
0.0 5
0.0
h
0.0
0.0 5
0.1
0.1 5
0.2
0.2 5
0.3
d
0.06
0.0 5
0.04
0.03
0.02
0.0 1
T ime (s)

(c)

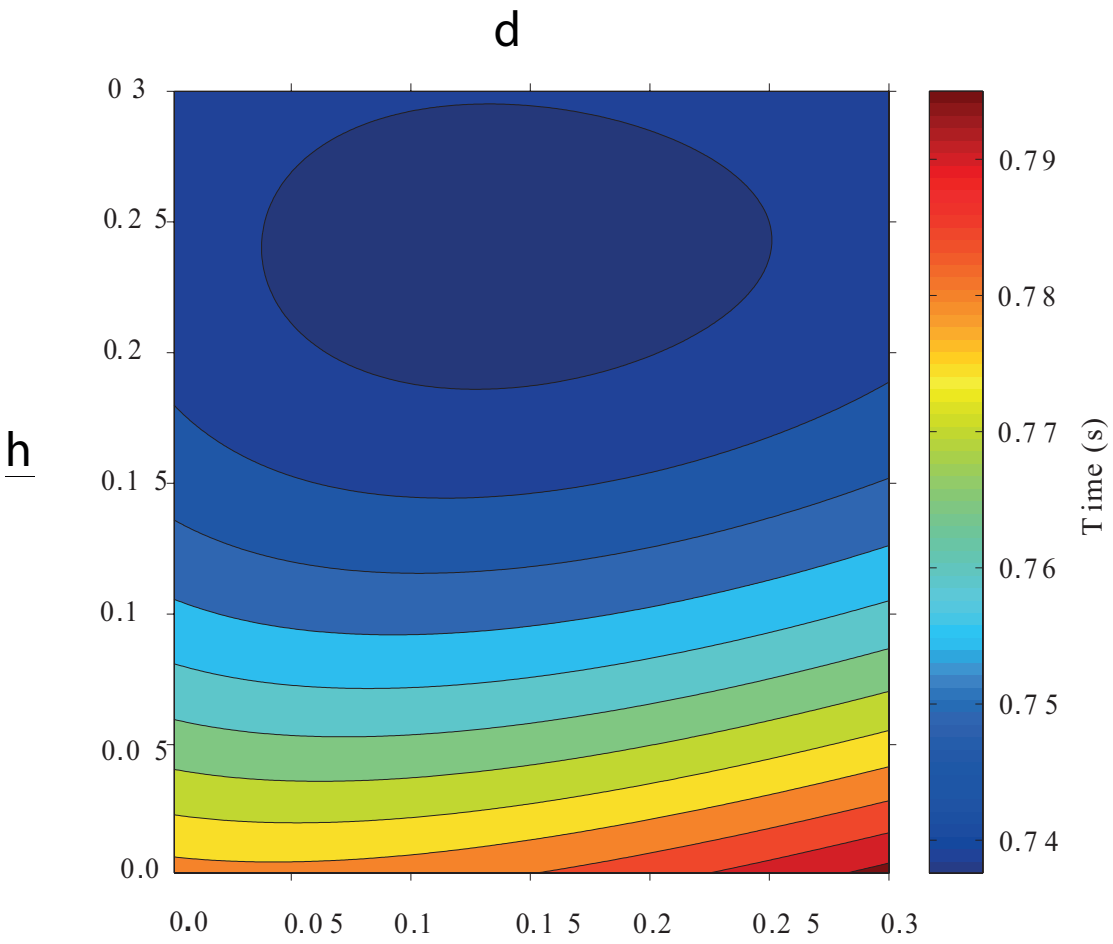
d
h
0 3
0.2 5
0.2
0.1 5
0.1
0.0 5
0.0
0.0
0.0 5
0.1
0.1 5
0.2
0.2 5
0.3
0.79
0.78
0.77
0.76
0.75
0.74
T ime (s)

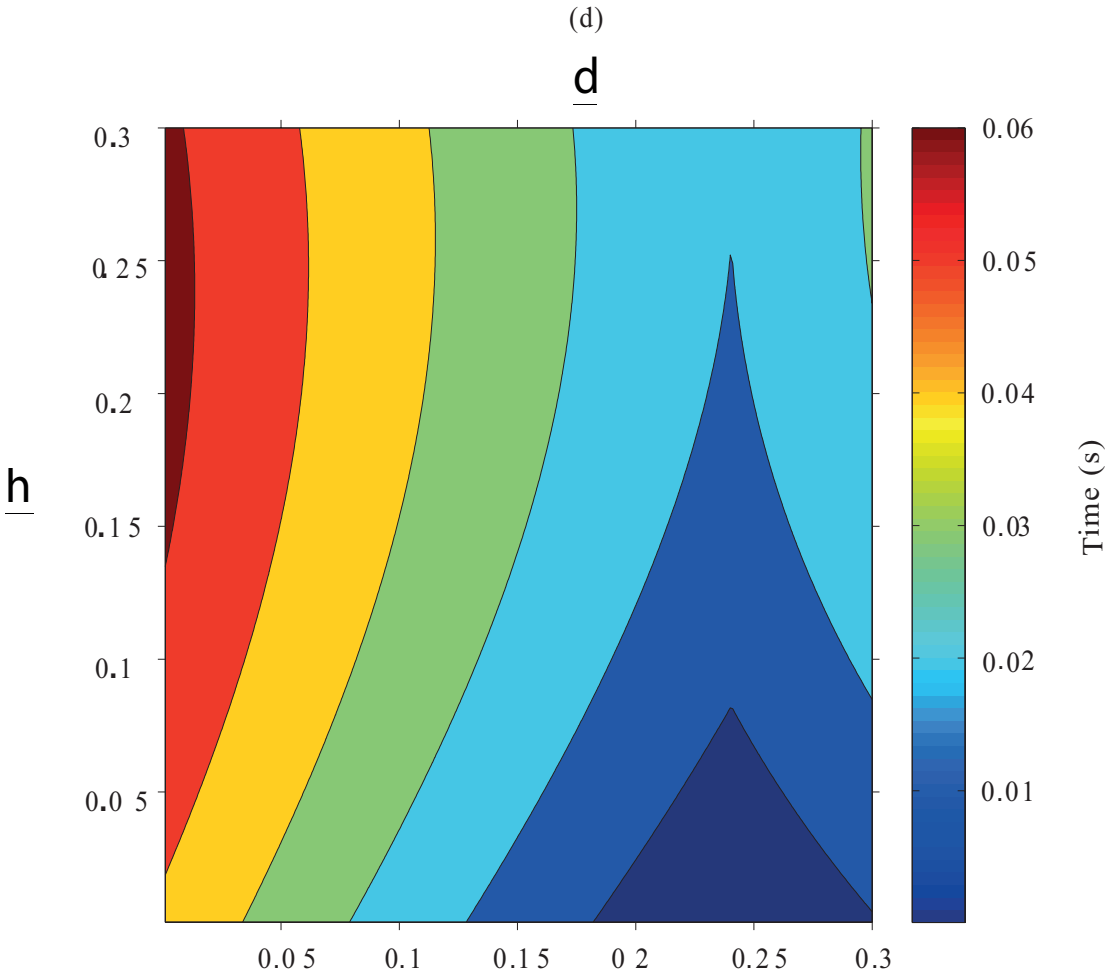

Figure 8. The influence of anisotropic parameters on the complex traveltimes of a vertical beam for a TTI medium. The starting point of the ray is at (6 km, 6 km), $\Delta\eta = 0.001$, and $\Delta\delta = 0.001$. The initial ray tube width is 300 m. Figures (a), and (c) show the influence of anisotropic parameters on the real part of the complex traveltimes, while Figures (b) and (d) show the influence of anisotropic parameters on the imaginary part of the complex traveltimes. The location for Figures (a) and (b) is (2 km, 2 km). The location for Figures (c) and (d) is (4 km, 4 km).

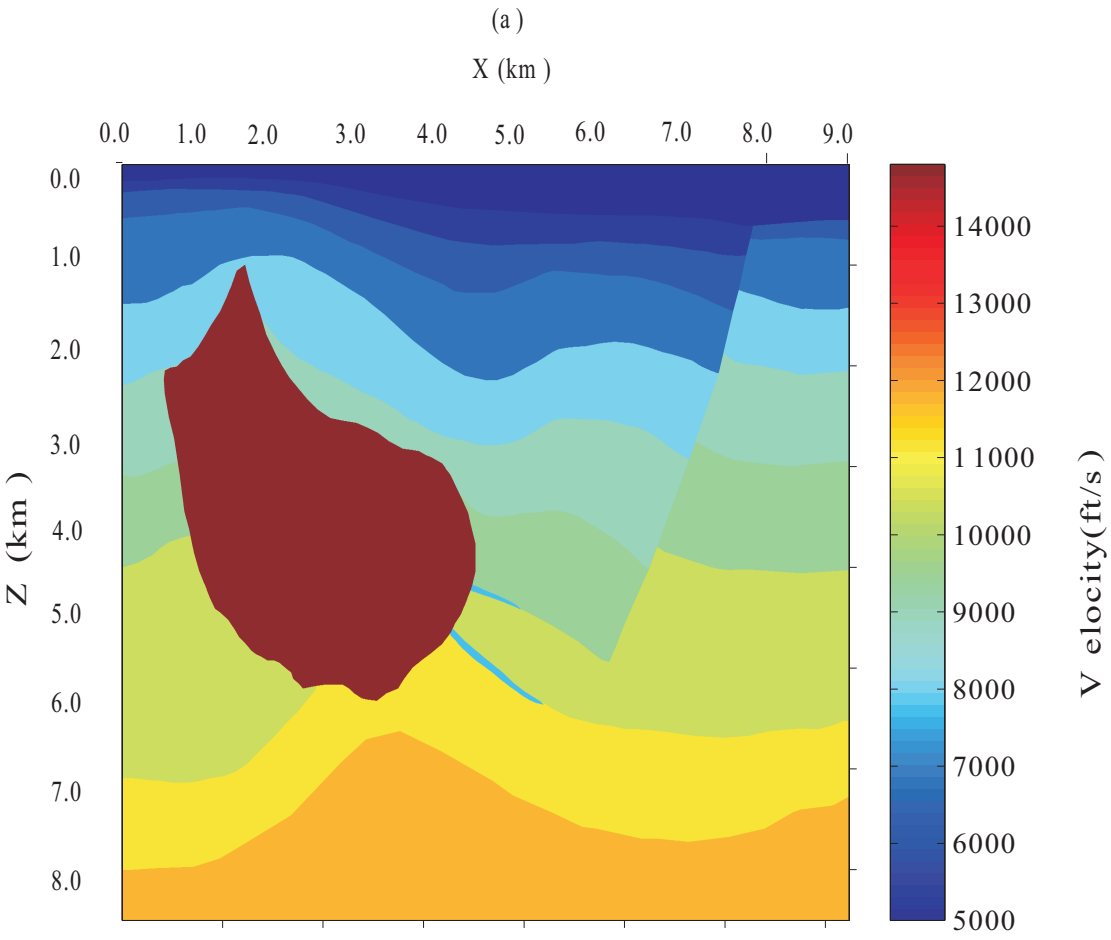
(a)
X (km)
0.0
1.0
2.0
3.0
4.0
5.0
6.0
7.0
8.0
9.0
Z (km)
0.0
1.0
2.0
3.0
4.0
5.0
6.0
7.0
8.0
14000
13000
12000
11000
10000
9000
8000
7000
6000
5000
Velocity(ft/s)

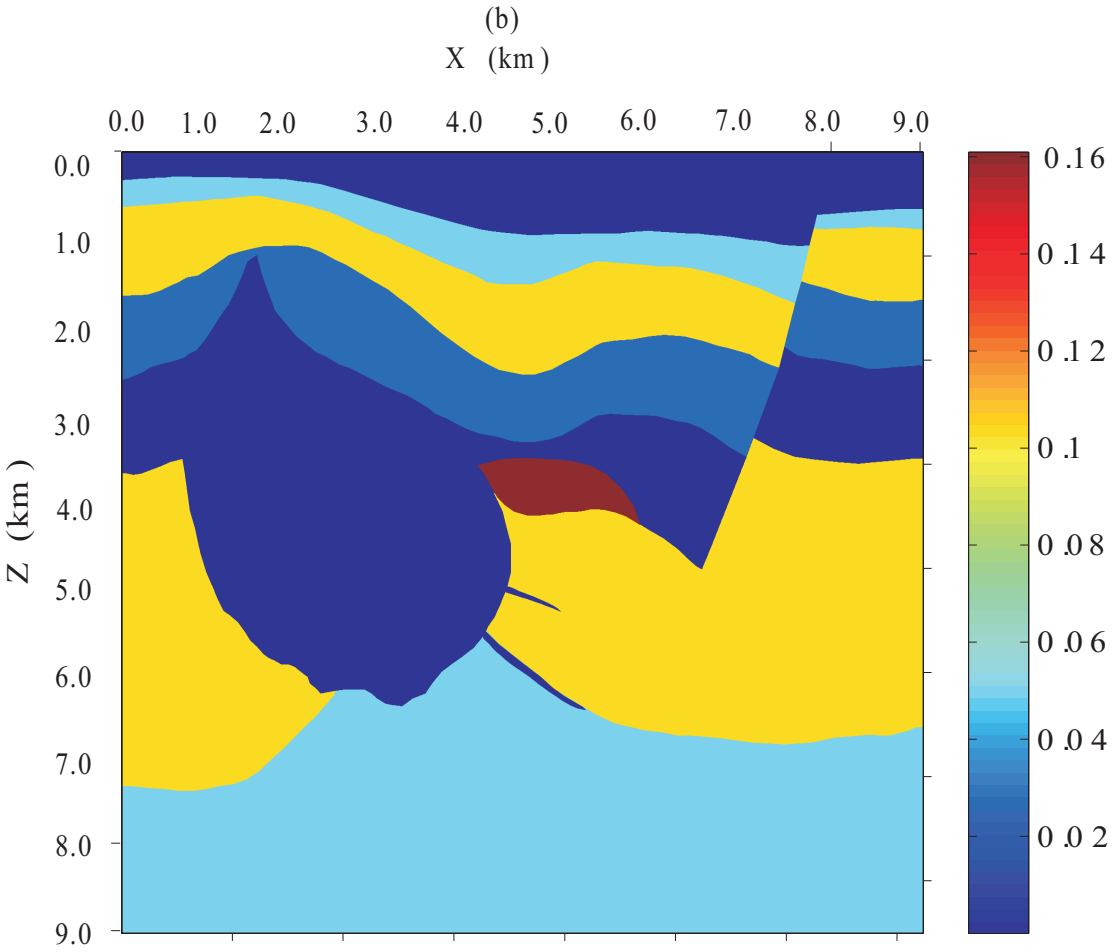
(b)
X (km)
0.0
1.0
2.0
3.0
4.0
5.0
6.0
7.0
8.0
9.0
Z (km)
0.0
1.0
2.0
3.0
4.0
5.0
6.0
7.0
8.0
9.0
0.16
0.14
0.12
0.1
0.08
0.06
0.04
0.02

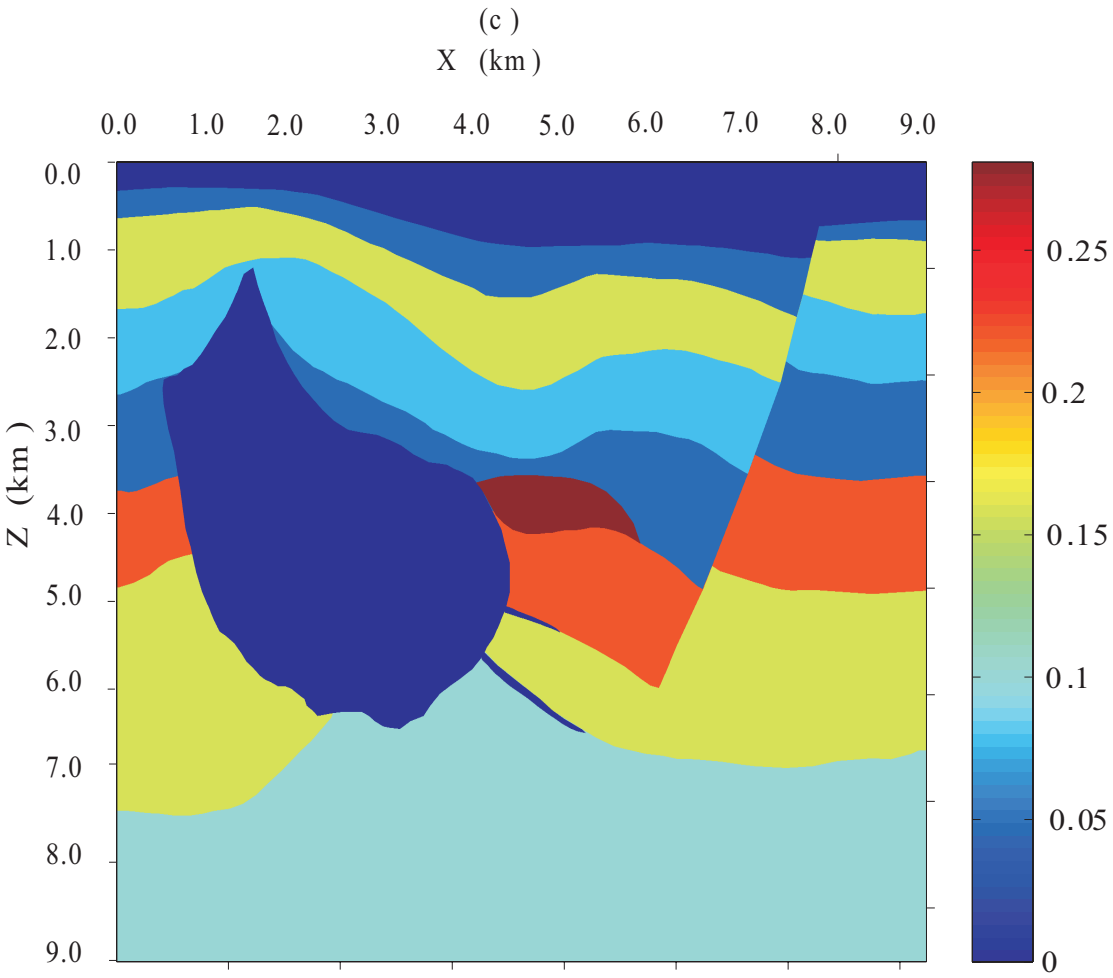
(c)
X (km)
0.0 1.0 2.0 3.0 4.0 5.0 6.0 7.0 8.0 9.0
Z (km)
0.0 1.0 2.0 3.0 4.0 5.0 6.0 7.0 8.0 9.0
0.25
0.2
0.15
0.1
0.05
0

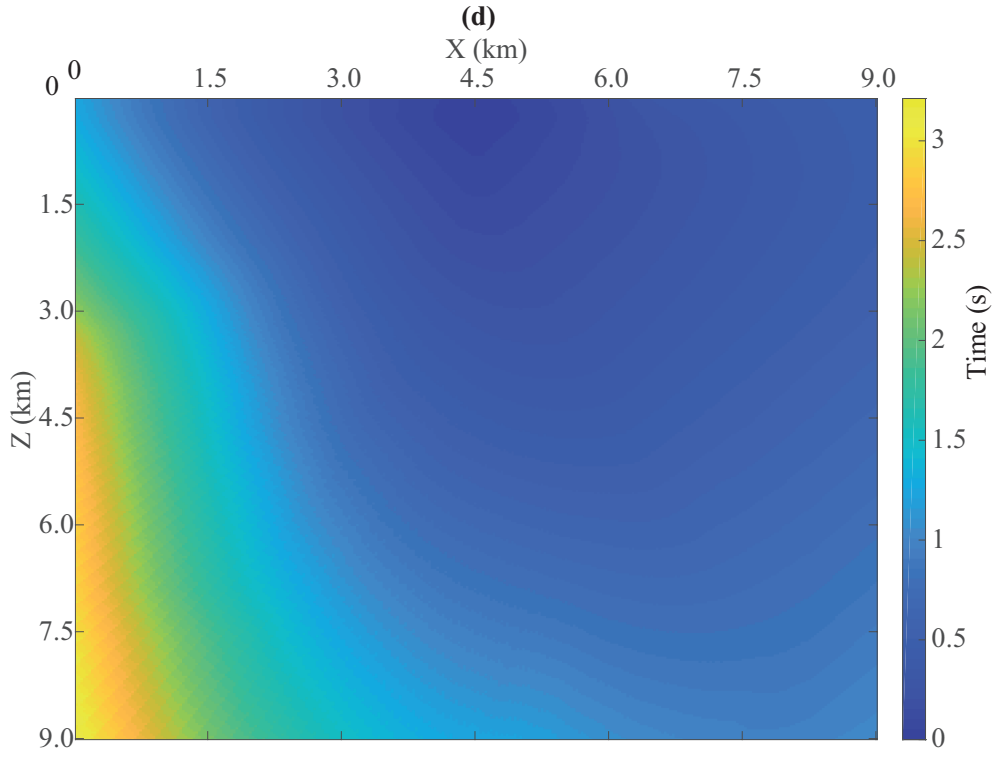
(d)
X (km)
0 1.5 3.0 4.5 6.0 7.5 9.0
Z (km)
0 1.5 3.0 4.5 6.0 7.5 9.0
3
2.5
2
1.5
1
0.5
0
Time (s)

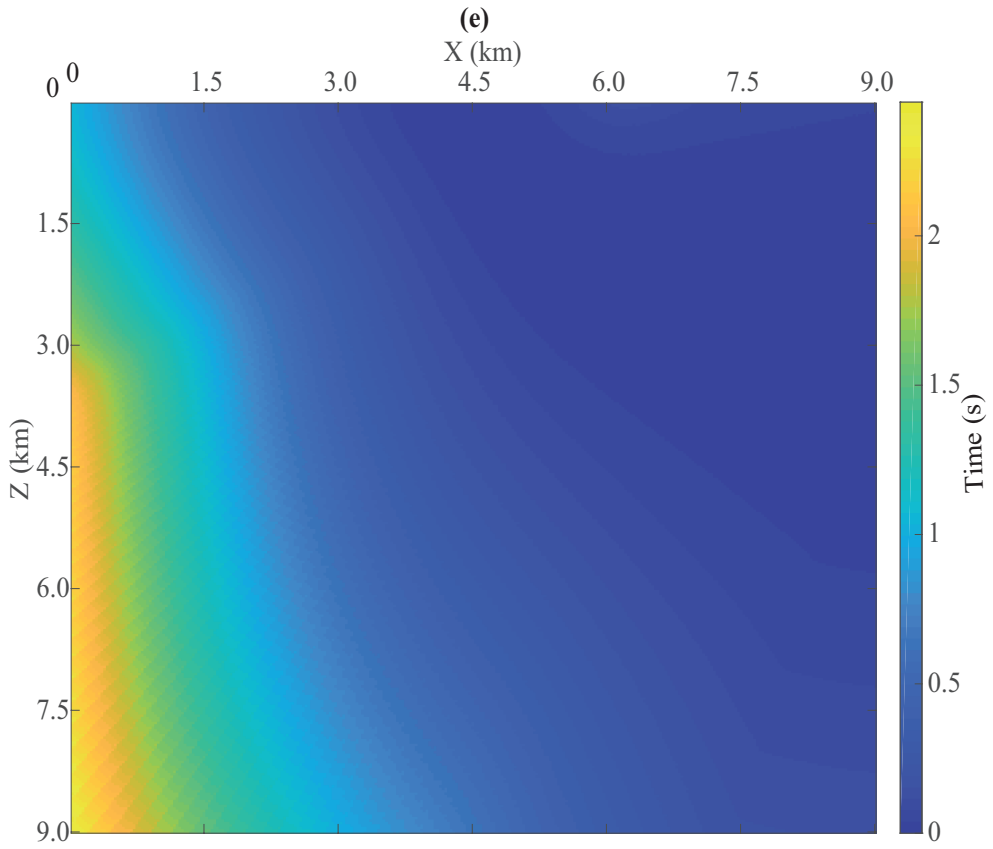

Figure 9. The complex traveltimes associated with a tilted ray for a VTI medium. The size of the model is (9 km, 9 km), which is based on the same model used in Figure 11 (Huang et al., 2018b). The initial angle of the central ray is $\theta = 60^{\circ}$. The starting point of the central ray is at (4.5 km, 300m), and the initial beam width is 500 m. Plot (a) shows velocity model, plot (b) shows δ model, plot (c) shows ε model, plot (d) shows the real part of the complex traveltimes and plot (e) shows the imaginary part of the complex traveltimes.